U.PORTO

FACULDADE DE FARMÁCIA
UNIVERSIDADE DO PORTO

Synthesis of new bioactive compounds for industrial application

Mestrado Integrado em Ciências Farmacêuticas

Project I Report

Ana Rita Couto Ribeiro Tavares

2017/2018

Faculdade de Farmácia da Universidade do Porto

Synthesis of new bioactive compounds for industrial application

Project I

2017/2018

Author: Ana Rita Couto Ribeiro Tavares

Advisor: Professora Doutora Marta Ramos Pinto Correia da Silva

Co-advisor: Mestre Ana Rita Conceição Neves

Date of evaluation: _____/_____/_____

Evaluators:

_____
_____
_____
_____
_____
_____

Classification:

_____

This work was developed in Laboratório de Química Orgânica e Farmacêutica, Departamento de Ciências Químicas, Faculdade de Farmácia da Universidade do Porto. This work was supported through national funds provided by FCT/MCTES - Foundation for Science and Technology from the Minister of Science, Technology and Higher Education (PIDDAC) and European Regional Development Fund (ERDF) through the COMPETE – Programa Operacional Factores de Competitividade (POFC) programme, under the projects PTDC/MAR-BIO/4694/2014 (reference POCI-01-0145-FEDER-016790; Project 3599 – Promover a Produção Científica e Desenvolvimento Tecnológico e a Constituição de Redes Temáticas (PPCDT)) and PTDC/AAG-TEC/0739/2014 (reference POCI-01-0145-FEDER-016793; Project 9471 – Reforçar a Investigação, o Desenvolvimento Tecnológico e a Inovação (RIDTI)) in the framework of the programme PT2020.

Part of the work concerning this report has been published as:

Abstracts in conference proceedings:

Tavares, A.R.; Neves, A.R.; Sousa, E., Pinto; M.M., Correia-da-Silva, M. Synthesis of a new xanthone by "click chemistry". 11th Meeting of Young Researchers of University of Porto (IJUP18), 2018, 14125.

Poster communication:

Tavares, A.R.; Neves, A.R.; Sousa, E., Pinto; M.M., Correia-da-Silva, M. Synthesis of a new xanthone by "click chemistry". 11th Meeting of Young Researchers of University of Porto (IJUP18), Porto, Portugal, February 7-9, 2018.

ACKNOWLEDGEMENTS

Firstly, I would like to thank to my advisor, Professor Marta Correia da Silva, for this challenging and fulfilling opportunity, which allowed me to get new knowledge and to discover a new passion.

To Professor Madalena Pinto, I would like to thank for allowing me to work in Laboratório de Química Orgânica e Farmacêutica.

To my co-advisor, M.Sc. Ana Rita Neves, I do not have enough words to say how grateful I am. For the patience, kindness, support, knowledge exchange and more, I am very thankful.

To Professor Emília Sousa, I would like to thank for being a great teacher throughout the course.

In addition, I would like to thank to Drª Sara Cravo and Gisela Adriano for the technical support and kindness.

To all my lab partners, the LQOF researchers Francisca Carvalhal, Cátia Vilas Boas, Álvaro Magalhães, João Ribeiro, Fernando Durães, and Daniela Loureiro, and to my Project I colleagues, Patrícia Barbosa, Pedro Vilares, Ana Rita Franco and Patrícia Marques for the support and for the friendly environment.

At last, to all my dearest friends and family, for the support, strength and encouragement.

LIST OF FIGURES

LIST OF SCHEMES

LIST OF TABLES

SUMMARY

ABSTRACT

Antifouling strategies have been used since the early Phoenicians. Over the years, most of these strategies were restricted due to their toxicity to marine environment and, consequently, to public health. The synthesis of nature-inspired compounds with antifouling properties is a great alternative to the isolation of natural compounds and to assure commercial supplies.

Sulfation is a metabolic strategy used by living organisms to originate non-toxic derivatives. In this direction, the synthesis of compounds with sulfate groups was planned in LQOF as a possible non-toxic alternative to current biocides. Furthermore, as recent studies in fouling-resistant coatings showed that combining hydrophobic molecules to hydrophilic polysaccharides creates amphiphilic coatings with inert properties reducing the interfacial bond of biofouling organisms to the surface, glycosylation of small molecules was also planned. A triazole group was selected to establish the linkage between the small molecules and glycoside moieties to mimic triazole-based biocide properties.

In this work, scale up synthesis of two previously obtained antifouling compounds, gallic acid persulfate and triazole-linked xanthone glucoside was planned. Furthermore, in order to understand the influence of the saccharidic moiety on the antifouling activity, the synthesis of triazole-linked xanthone cellobioside was also planned.

Overall, five compounds were synthesized, one of which were new compounds. Sulfation of gallic acid and the syntheses of triazole-linked xanthone glucoside and cellobioside by “click chemistry” were performed under microwave irradiation to achieve short reaction times and high yields. Structural elucidation of all compounds was established by infrared and ^{1}H and ^{13}C nuclear magnetic resonance.

Future work will consist in the evaluation of the antifouling activity of the new triazole-linked xanthone cellobioside to understand the influence of the saccharide moiety on the antifouling activity.

Keywords: antifouling, natural compounds, sulfation, gallic acid, xanthone, polysaccharides, triazole, “click chemistry”.

ABBREVIATIONS AND SYMBOLS

δ - Chemical shift

^{13}C NMR - Carbon nuclear magnetic resonance

^{1}H NMR - Proton nuclear magnetic resonance

ACN - Acetonitrile

AF - Antifouling

brs - broad singlet

$CDCl_3$ - Deuterochloroform

CuAAC - Copper (I)-catalyzed azide-alkyne cycloaddiction

d - Doublet

dd - Double doublet

DMA - *N*,*N*-Dimethylacetamide

DMF·SO_3 - *N,N*-Dimethylformamide sulfur trioxide adduct

DMSO-d_6 - Dimethylsulfoxide-d_6

EPS - Extracellular polymeric substances

IR - Infrared

***J* -** Coupling constant

m - Multiplet

MeOH - Methanol

MW - Microwave

NaAsc - Sodium ascorbate

NMR - Nuclear magnetic resonance

PTC - Phase transfer catalyst

Py·SO_3 - Pyridine sulfur trioxide adduct

s - Singlet

S_N2 - Bimolecular nucleophilic substitution

t - Triplet

TBAB - Tetrabutylammonium bromide

TBT - Tributyltin

TEA·SO_3 - Triethylamine sulfur trioxide adduct

THF - Tetrahydrofuran

TLC - Thin layer chromatography

1. INTRODUCTION

1.1. The Marine Biofouling Process

Biological fouling, commonly referred as biofouling, is the accumulation of unwanted biological matter on surfaces, with biofilms created by microorganisms and macroscale biofouling formed by macroorganisms [1]. Biofouling process occurs in many environments and in diverse ways. For example, medical biofouling only includes the development of biofilms in medical devices but industrial and marine biofouling are a combination of micro and macrofouling [1].

Marine fouling organisms are divided into two categories: microfoulers and macrofoulers. The first category corresponds to microfouling or biofilm organisms, which are bacteria and diatoms. Microfoulers attach to surfaces and begin the biofouling process, under favourable conditions, with the production of a ubiquitous biofilm. This sticky coating provides food and an interface for macrofouler organisms to attach, such as algae, barnacle, mussels, polychaete worms, bryozoans, and seaweed [2].

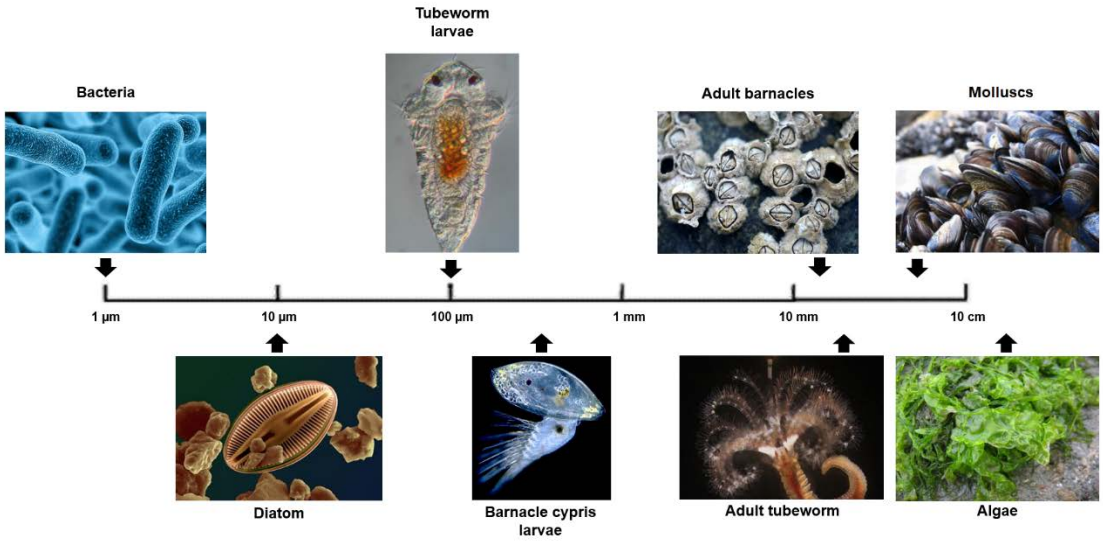

Figure 1 - Size comparison between micro and macrofouling organisms (adapted from [2]).

Marine biofouling is a dynamic process described in four phases. Since marine biofouling occurs in an aqueous solution, the properties of the fluid mediate the interaction between the organisms and the materials [3]. The process begins with ions and water adsorption to a surface to form an electric layer. Once surface electric charge is established, there is a conditioning film formation by

physical reactions between the surface and organic materials such as proteins, polysaccharides and proteoglycans [3, 4]. This phase is short lasting a minute.

The protein layer provides a surface for the settlement of bacteria and, consequently, for the development of a biofilm. Bacterial colonization involves two steps: reversible adsorption and irreversible adhesion. The reversible adsorption is affected by physical reactions such as electrostatic interaction, gravity and water flow. After the initial reversible absorption, irreversible adhesion occurs through biochemical effects such as temporarily adherence to the surface by extracellular polymeric substances (EPS), such as, glucose and fructose-based polysaccharides. The biofilm is formed when the bacterial communities secrete more EPS. The EPS coating is both an adhesive and protective layer that modulates the diffusion of molecules in the biofilm. Consequently, bacteria in biofilms are more resistant to antibiotics and antibacterial agents. Homologous and mixed species with proteins and enzymes form a complex but functional community. After biofilm maturation, bacteria disperses into the water to expand the species [3, 4].

Diatom adhesion is a more complicated process because, since diatoms lack flagella, they cannot actively approach the surface, but passively land through electrostatic interaction. After landing, diatoms actively form the reversible and irreversible attachment by secreting large amount of EPS. The EPS produced by diatoms is composed of carboxylated or sulfated acidic polysaccharides and proteoglycans. Those are responsible for the adhesion, diatom gliding and the cross-linking stabilization of the biofilm matrix [4].

Biofilms facilitate the settlement of secondary macroorganisms, such as spores of macro algae, barnacle larvae, bryozoans and molluscs [3]. The interaction between biofilm and secondary colonizers is a complex interplay of surface chemistry, micro-topography and microbial products. It is believed that microorganisms (bacteria and diatoms) produce low molecular metabolites to repel some macroorganisms. The adhesion mechanisms are different in specific organisms. For example, barnacles have cyprid that adhere by secreting granulated cement containing high concentrations of polymerized proteins [4]. Another example is Ulva spores, which are very abundant and adaptable in different seawater environments. Ulva spores adhere strongly to a surface by secreting glycoproteins [4].

Overall, the biofouling process is complete after two or three weeks, when it evolves into a complex biological community [4].

The undesirable attachment of macrofoulers organisms compromises exponentially the functionality of ships and structures immersed in seawater such as buoy sensors and harbour installations [2]. The severity of biofouling depends on various parameters presented in **Figure 2**. Generally, it is accepted that in tropical areas with high water temperature, biofouling communities are conditioned in their reproduction and growth [4]. During seasonal changes, biofouling communities in tropical areas are more pronounced since the growth rates are fastest and larvae and propagules are abundant [5].

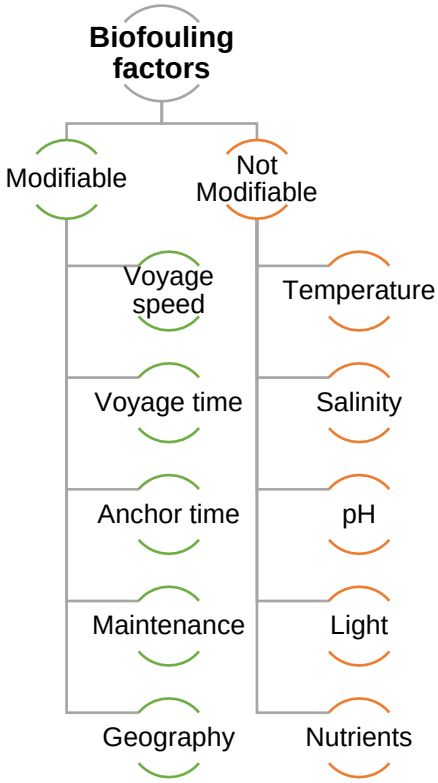

Figure 2 - Factors influencing the rate of biofouling.

The marine biofouling process is considered a global issue concerning serious ecological, economic, and health problems. Marine industry and biodiversity of marine ecosystems are the most affected. Both have direct and indirect effects in public health such as the spread of pathogens [1]. To understand the importance of AF strategies it is necessary to reveal the problematic associated with marine biofouling (**Figure 3**).

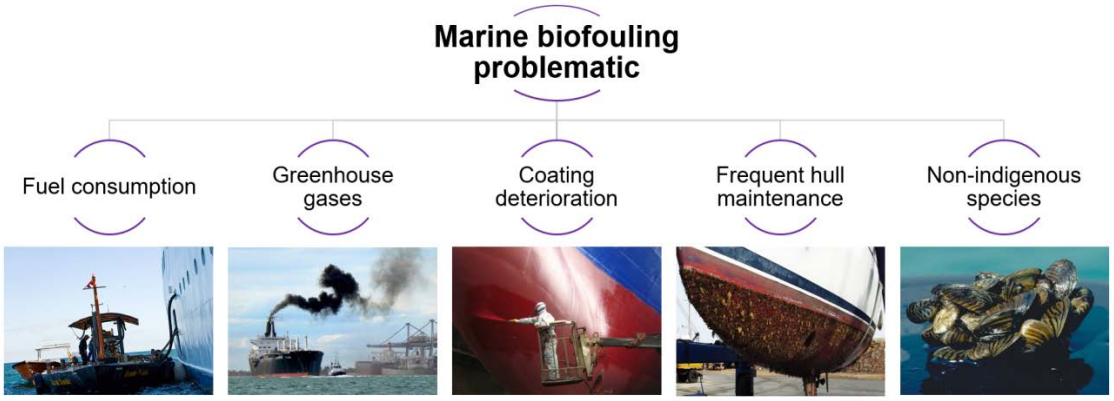

Figure 3 - Problems associated with marine biofouling.

Marine biofouling is a particular problem for underwater structures, colonizing pipelines, cables, fishing nets, bridge pillars, ship's hull, oil installations, platforms and marinas [4]. Regarding the side effects of ship hull biofouling, some can be listed. Firstly, fuel consumption increases about 40% due to increased frictional resistance and, consequently, shaft power to reach a certain speed. In addition, some coatings make the hull rougher and the ship heavier, contributing to the problematic. Even biofilms can lead to a significant increase up to 20% in resistance and powering [4, 6]. Furthermore, emissions of greenhouse gases such as CO_2, NO and SO_2 are directly proportional to the amount of fuel consumption, contributing to global warming [1]. Secondly, as the protective coating surface deteriorates, ship's hull is more susceptible to corrosion by acid producing bacteria in the biofilm and discoloration [1, 4]. At last, the total cost for ship operations associated with or resulting from hull biofouling arises due to operating, supply, maintenance or modernization. Moreover, there is an ecological impact associated since the cleaning process generates a large number of toxic substances that are discharged into the ocean [4, 6].

The transport of non-indigenous biofouling species between bio-geographic regions in various vectors such as ballast tanks or ship's hull is a major threat to the conservation of biodiversity and contribute to environmental change [7]. The most potential invasive species who set a reproductive population in the host environment become invasive and out compete the native species [7]. Data showed that the rate of bio-invasions is continuing to increase at an alarming rate and new areas are being invaded [8]. Furthermore, invasive marine species have a negative impact on human health and decrease economic

production of activities based on marine environments and resources such as fisheries, aquaculture, tourism and marine infrastructure [7]. Also, there are costs associated to management, eradication, and control measures of evasive species [8].

1.2. Antifouling Strategies

An ancient civilization originated in the Eastern Mediterranean, the Phoenicians, was credit for the first advance in antifouling (AF) technology by simply using a form of lead and cooper sheets on their wooden boats (**Figure 4**) [9]. Until the 20th century, coatings containing cooper, arsenic, and mercury were highly applied to vessel hulls [9].

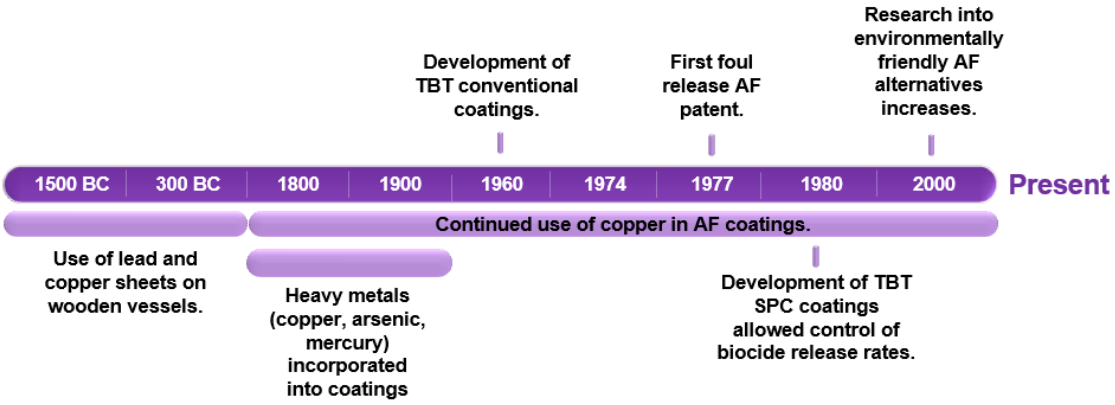

Figure 4 - Historical timeline of AF strategies [9].

Before the 21th century, traditional chemical methods were widely used, mainly organotin compounds. For example, tributyltin (TBT) oxide, TBT fluoride, and their derivatives proved to be effective against a wide range of biofouling species. These compounds are classified as potent biocides or fungicides that can inhibit the growth of most biofouling organisms at a low concentration [4, 9]. The use of TBT paints by private and commercial users accelerated greatly in the 1970s, and at the same time, the first TBT effects were observed on non-target organisms. Prolonged exposure to sub-lethal concentrations of TBT caused malformations in the reproductive system, for example, the development of male sexual structures in females, known as imposex [10]. In 1971, the phenomenon was first described in American mud-snail (*Nassarius obsoletus*) and, around that time, it was recorded the appearance of a penis in female dogwhelks (*Nucella lapillus*) [11]. Only in early 1980s the connection between TBT and these effects

was made [10]. **Figure 5** provides a brief restriction' summary regarding organotin compounds [12].

The restriction of the use of TBT, mercury and arsenic made possible the reuse of cooper-based paints and/or the use of new paints incorporating high booster concentration of cooper. Currently, most of tin-free AF paints contain cooper, which target specific biofouling organisms, including microorganisms, fishes, and macroalgae. Therefore, it is necessary to add booster biocides highly toxic to macroalgae, barnacles and bryozoans, to lower cooper concentrations [4, 9]. Ideally, a good AF biocide is effective in preventing biofouling of the painted surface without persisting at higher concentrations that may cause negative environmental effects. This can be achieved by rapid release from the surface or specifically act on the target [13]. In the 21th century, various projects aimed to understand the toxic effects and possible restrictions of AF biocides (**Table 1**) [9, 13-15].

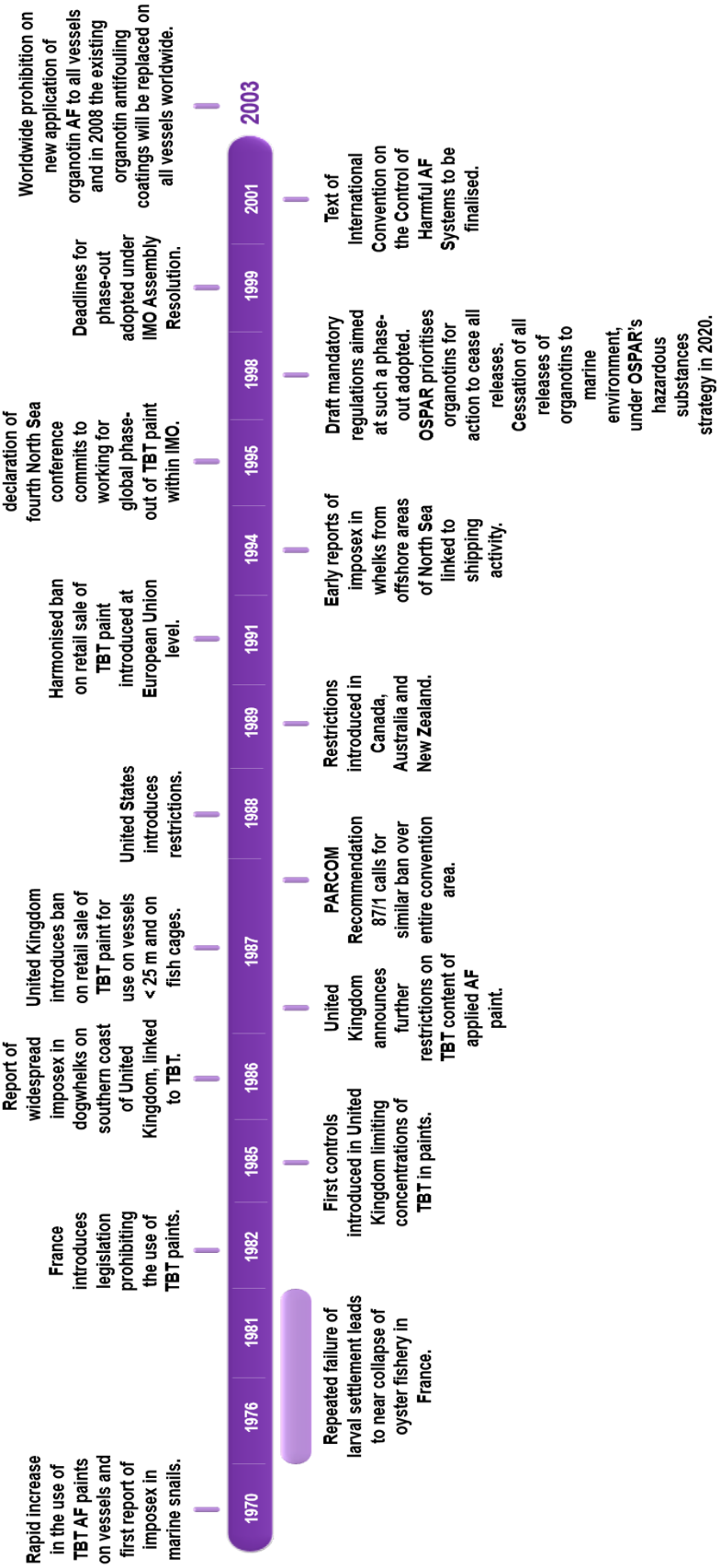

Figure 5 - Historical timeline of organotin compounds restrictions [12].
AF: Antifouling. TBT: tributyltin.

Table 1 - AF biocides applications, toxic effects and approval or restriction status [9, 13-15].

AF Biocide	Chemical class	Application	Toxic effects	Approval or Restriction
Copper	Organometallic salt	Added as a thiocyanate, copper metal oxide or sulphide.	Toxic for algae and molluscs, suitable for seawater, and not recommended for freshwater. Effect limited to quality and environmental conditions.	First successful AF sheathing. No global restriction.
Zinc pyrithione	Organometallic salt	Most popular surrogate antifouling biocides. Widely used as algaecide, bactericide and fungicide.	Highly toxic to aquatic plants and animals.	Approved in UK and US for pleasure boats. No global restriction.
Irgarol 1051	*s* -Triazine	Herbicide used in concert with copper to control fouling on boat hulls.	Disturb electron transfer process within Photosystem-II. Fatal effects on marine life.	Approved for larger vessels by 98/8/EE directive implementation Restricted in UK
Sea Nine 211	Isothiazolone	Present in commercial paints as a main or booster biocide (1–3%).	Acute toxicity to a wide range of aquatic organisms. No chronic toxicological effects.	Approved in US Restricted in UK
Diuron	Phenylurea	Pre- and post-emergent weed control in both crop and non-crop areas, to prevent mildew growth, as an algaecide in antifouling paints, and in commercial fish production and aquariums.	Toxic for reproduction of green freshwater alga *Scenedesmus vacuolatus*. Affect planktonic and microalgae by reducing chlorophyll *a* levels. Toxic to certain bacterial species.	Restricted by 98/8/EE directive implementation
Dichlofluanid	Organochlorine	Potential to bioaccumulate.	Low toxicity.	No global restriction.
Chlorothalonil	Organochlorine	Present in antifouling paints, mainly as a booster biocide. First in use as a broad-spectrum fungicide in agriculture, silviculture, and urban settings.	Acute toxicity to fish depending on the species and the exposure conditions. Bioaccumulate in tissue of fish such as willow shiner (*Gnathopogon caerulescens*) and carp (*Cyprinus carpio*).	Restricted by US EPA

Currently, there are nontoxic solutions for the problems originated by marine biofouling. Nevertheless, cooper-containing coatings are considered a transition between toxic and non-toxic coatings [12]. Nowadays, investments are made in research and development of non-toxic alternatives such as foul-release coatings that incorporate silicone elastomers, waxes or silicone oils, and “natural” coatings that contain AF compounds from algae and other marine organisms [12].

Several studies demonstrate that some marine organisms stay relatively free from biofouling, suggesting that those organisms have AF strategies [16]. In most cases, marine species rely on a combination of physical, chemical and biological strategies. Many organisms such as macroalgae, sponges and corals excrete secondary metabolites to repel biofouling organisms and/or associate to specific microorganisms to prevent colonization of biofouling organisms [16]. These natural biocides generally have a more intricate and specific AF mechanism compared to conventional biocides [17]. For example, furanon, obtained from a red seaweed, is 100 times more effective than TBT, and bufalin, a toad poison, is 100 times more toxic than TBT and 6000 times more effective against barnacles [17]. However, only a few amounts of marine-based bioactive compounds can be extracted, making it difficult to obtain the minimum requirement needed to undergo toxicological assays [18]. Other barriers are shown in **Figure 6** [18].

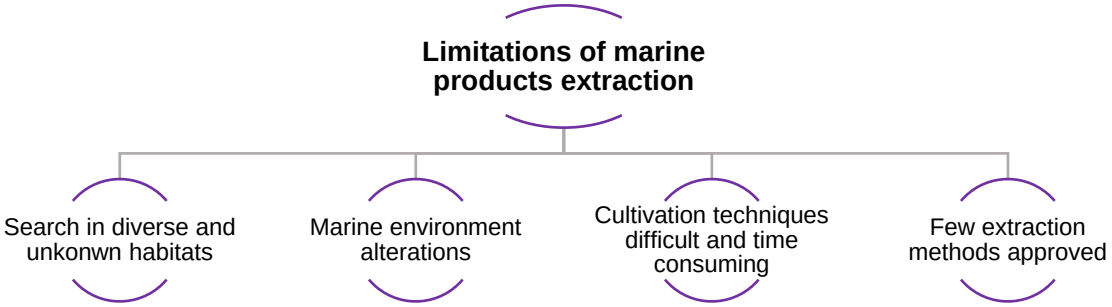

Figure 6 - Limitations of marine products extraction.

Total synthesis or semi synthesis is a more practical and economic answer to produce high amounts of simple compounds or to chemically modify available compounds into the desired one with AF properties inspired in Nature [19].

The synthesis of natural products with a sulfated moiety is a possible non-toxic and eco-friendly alternative. Since sulfation of biomolecules is a metabolic strategy used in most marine organisms, no harmful effects to the marine ecosystem are expected [20]. In the marine environment, sulfated metabolites have been identified as storage forms for more active metabolites that only upon enzymatic cleavage (sulfatase), the “activated” form develops its specific properties [21]. For example, zosteric acid is a sulfated phenolic acid isolated from the sea grass *Zostera marina* [22]. In the last decade, this secondary

metabolite has attracted much attention due to its AF activity through biofilm inhibition. However, studies showed that *para*-coumaric acid, obtained by bioactivation of zosteric acid (**Scheme 1**), has antimicrobial properties further more intense [21].

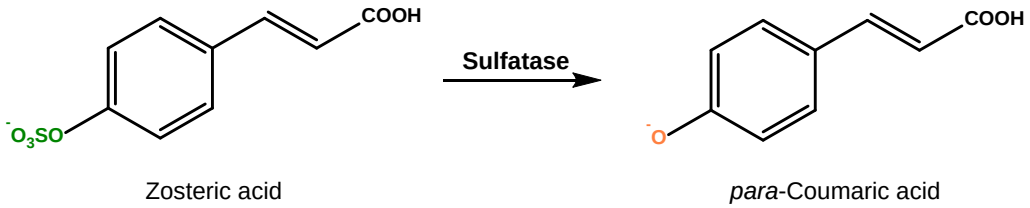

Zosteric acid — *para*-Coumaric acid

Scheme 1 - Enzymatic cleavage by sulfatase of zosteric acid to para-coumaric acid.

Recent studies of fouling-resistant coatings showed that hydrogels such as ethylene glycol polymers have the ability to store water, holding the attachment of fouling organisms [23, 24]. Despite the AF properties, ethylene glycol polymers suffered rapid degradation, so new hydrophilic alternatives are in search. For example, polysaccharides as hyaluronic acid and alginic acid are highly hydrated and resist to adhesion [23]. However, hydrophilic coatings have showed to be unsuitable to be applied in the marine environment [23]. Currently in study are amphiphilic coatings, which incorporate some of the benefits of both hydrophobic and hydrophilic functionalities [24]. Combining incompatible block polymers, it is created a dynamic and compositional surface complexity that deters settlement stages of fouling organisms and reduces the interfacial bonding with adhesive polymers [24].

Inert surface coatings with amphiphilic properties can be obtained by combining hydrophilic polysaccharides as glucose with hydrophobic molecules as xanthones [23]. A triazole group establishes the linkage between the two moieties, in order to mimic potent triazole-based biocides [20]. The most promising triazole-based biocides lies in azole-metal coordination to Cu^{2+} (**Scheme 2 – A**), which is a potent AF biocide. Although copper is essential to many enzymes where redox reactions are the central function, high copper concentrations disrupt cell homeostasis by inactivating enzymes or precipitating cytoplasmic proteins into metal-protein aggregates, therefore maintaining its biocide properties [17]. The ion Cu^{2+} is reduced to solid copper due to reducers as Zn^{2+} present in sea water or ship's structure, resulting in corrosion. An AF

coating with a triazole moiety can absorb large amounts of naturally abundant cooper in the marine environment [17, 25]. The presence of Cu^{+} stabilizing ligands such as sulfur-containing ligands catalyses the reduction of Cu^{2+} to Cu^{+} (**Scheme 2 – B**) preventing corrosion by Cu^{2+} [17].

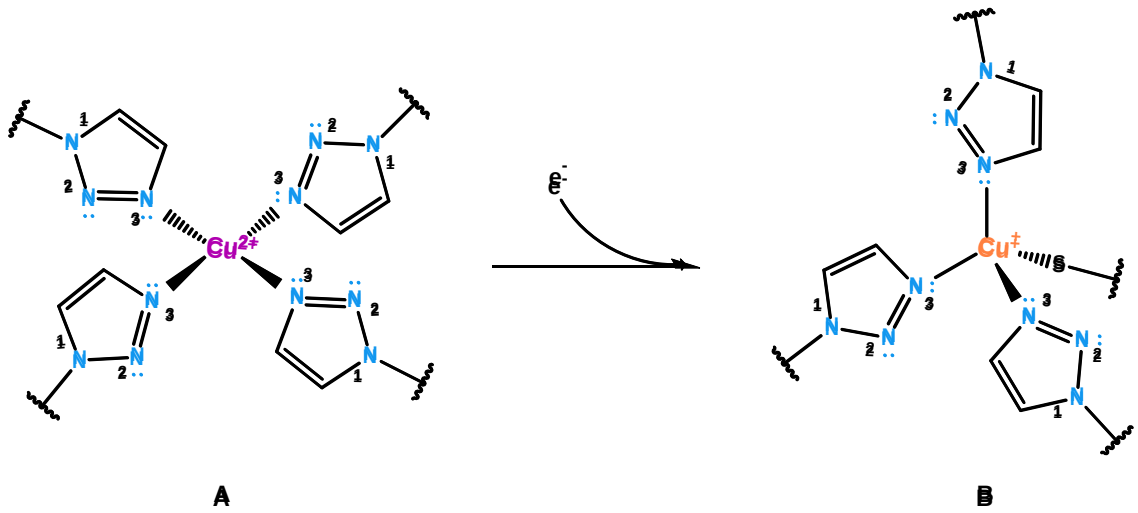

Scheme 2 - Mechanism of triazole-metal coordination to Cu^{2+} (**A**) and redox reaction (**B**), adapted from [17].

As potential AF agents, benzoic acid derivatives (ex. gallic acid) and xanthones linked to saccharides units (ex. glucose, galactose and rutinose) were sulfated and their effectiveness and ecotoxicity was assessed [20].

1.3. Aims

Previous work in our group showed that gallic acid persulfate (**Figure 7**) and 3,6-bis(triazole ethyl 2,3,4,6-tetra-*O*-acetyl-*β*-D-*O*-glucopyranosyl)-9*H*-xanthen-9-one (**Figure 7**) were active against the settlement of the mussel *Mytilus galloprovincialis*, a macrofouler, with an EC_{50} of 17.65 µM [20] and 9.89 µM (unpublished results), respectively. Regarding gallic acid persulfate it is worth to mention that gallic acid was not active against the settlement of the mussel *Mytilus galloprovincialis*, highlighting the importance of the sulfate groups for the AF activity. The goal of this work was to scale-up the synthesis of in-house compounds with AF activity and to synthesize acetosugar triazole-linked

xanthones with different sugar moieties to obtain in the future a structure-activity relationship.

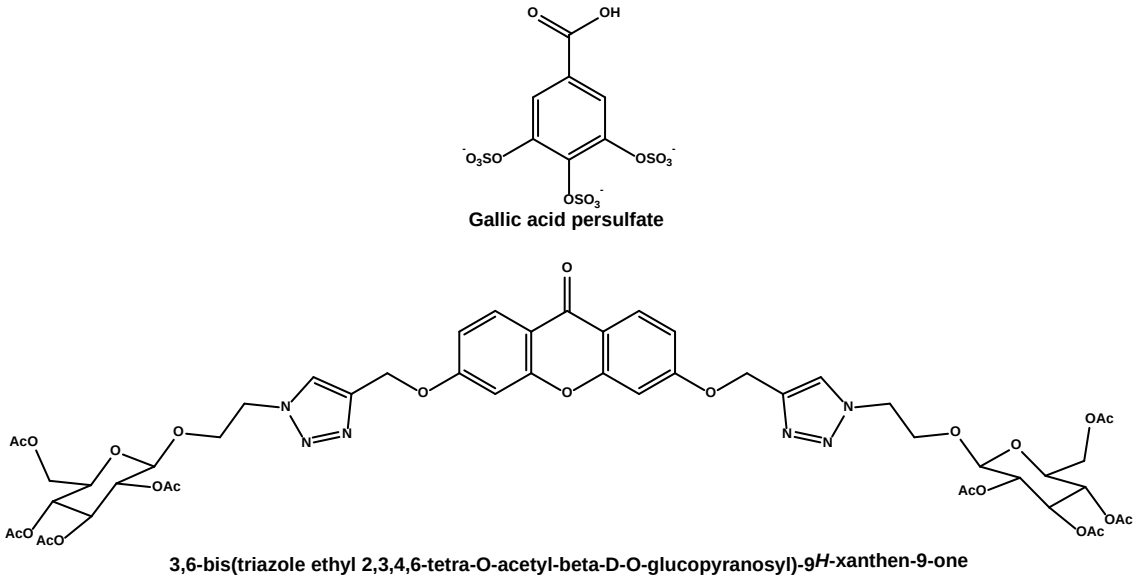

Figure 7 - Structure of gallic acid persulfate and 3,6-bis(triazole ethyl 2,3,4,6-tetra-*O*-acetyl-*β*-D-*O*-glucopyranosyl)-9*H*-xanthen-9-one.

Therefore, this project had the following specific goals:

1) The scale-up synthesis of previously synthesized compounds with AF activity
2) The synthesis of new celobiosyl-heptacetate triazole-linked xanthone using the CuAAC reaction.
3) The purification of the synthesized products to obtain pure compounds and characterize their structure using spectroscopic methods (infrared and ^{1}H and ^{13}C nuclear magnetic resonance).

2. RESULTS AND DISCUSSION

2.1. Synthesis

2.1.1. Gallic acid persulfate (2)

Gallic acid persulfate (**2**) was previously obtained in 36% yield by reacting gallic acid (**1**) with sulfur trioxide-triethylamine complex (TEA·SO_3) in *N*,*N*-dimethylacetamide (DMA) under microwave (MW) irradiation, at 100ºC for 1 hour (**Scheme 3**) [26]. In this project, several new conditions varying for example the solvent, temperature, reaction time, and the source of heat (conventional or MW) were considered in order to increase the yield (**Table 2**).

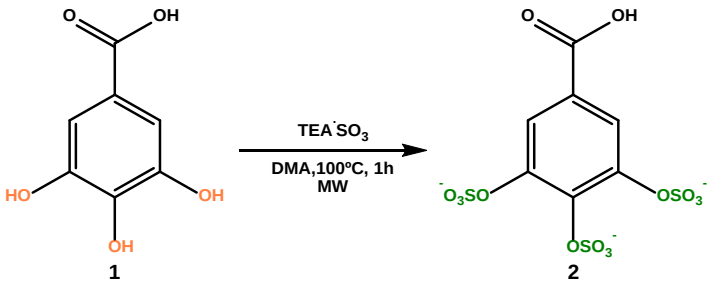

Scheme 3 - Synthesis of gallic acid persulfate (**2**).
TEA·SO_3: sulfur trioxide-triethylamine complex; DMA: *N*,*N*-dimethylacetamide.

The most commonly used reagents for the synthesis of polysulfated derivatives are complexes of sulfur trioxide (SO_3) with amines or amides, for example triethylamine(TEA)·SO_3, pyridine(Py)·SO_3 or dimethylformamide (DMF)·SO_3. Since SO_3 is a Lewis acid, the reactivity drifts from the different organic Lewis bases with which it is complexed [27]. The TEA·SO_3 has lower reactivity, whereas Py·SO_3 is reactive enough for aromatic sulfation and shows good stability at room temperature. However, when performing the sulfation of gallic acid with Py·SO_3 (entries 1 and 2, **Table 2**) reactions did not proceed efficiently when compared with reactions where TEA·SO_3 was used (entries 3-9, **Table 2**).

Table 2 - Different reagents and conditions for sulfation of compound **1**.

Entry	Reagent	Solvent	Reaction conditions	Reaction time	Results
1	Py·SO_3 (6 eq)	DMA	120˚C, reflux	2h30min	No product formed
2	Py·SO_3 (6 eq)	DMA	100˚C, MW, 200W(closed vessel)	30min	No product formed
3	TEA·SO_3 (9 eq)	DMA	100˚C, reflux	1h	No product formed

4	TEA·SO_3 (9 eq)	DMA	100˚C, MW, 200W (closed vessel)	1h	Three products formed and gallic acid was completely consumed
5	TEA·SO_3 (3 eq)	ACN	65˚C, reflux	1h	Reaction evolved incompletely: one product formed but gallic acid was not completely consumed
6	TEA·SO_3 (9 eq)	ACN	100˚C, reflux	1h	Three products formed and gallic acid was completely consumed
7	TEA·SO_3 (3 eq)	ACN	74˚C, MW, 200W (opened vessel)	1h	Two products formed but gallic acid was not completely consumed
8	TEA·SO_3 (3 eq)	ACN	100˚C, MW, 200W (closed vessel)	1h	Three products formed (one of them in small quantity) but gallic acid was not completely consumed
9	TEA·SO_3 (9 eq)	ACN	100˚C, MW, 200W (closed vessel)	1h	Three products formed (one of them in larger quantity) and gallic acid was completely consumed

Although the spot corresponding to gallic acid persulfate (**2**) appeared during reaction control with thin layer chromatography (TLC), actually, after purification, it was obtained a gallic acid disulfated only in positions 3 and 5, gallic acid 3,5-disulfate (**3**, **Figure 8**).

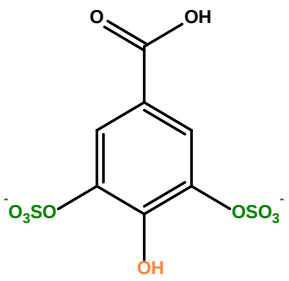

Figure 8 - Structure of gallic acid 3,5-disulfate (**3**).

2.1.2. 3,6-Dihydroxy-9*H*-xanthen-9-one (5)

3,6-Dihydroxy-9*H*-xanthen-9-one (**5**) was synthesized by dehydration of 2,2',4,4'-tetrahydroxybenzophenone (**4**), at 220ºC (**Scheme 4**) [29].

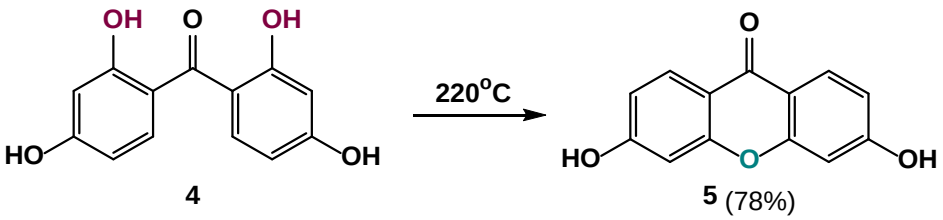

Scheme 4 - Synthesis of 3,6-dihydroxy-9*H*-xanthen-9-one (**5**).

Intramolecular cyclization allowed the synthesis of the xanthone core with two hydroxyl groups in positions 3 and 6 which it is not commercially available. The reaction occurred at high temperature with no solvent or catalyst resulting in the release of one water molecule per molecule of xanthone.

2.1.3. 3,6-Bis(prop-2-yn-yloxy)-9*H*-xanthen-9-one (7)

3,6-Bis(prop-2-yn-yloxy)-9*H*-xanthen-9-one (**7**) was synthesized reacting propargyl bromide (**6**) with 3,6-dihydroxy-9*H*-xanthen-9-one (**5**), in the presence of tetrabutylammoniun bromide (TBAB), in acetone, at 60°C, for 5 hours (**Scheme 5**).

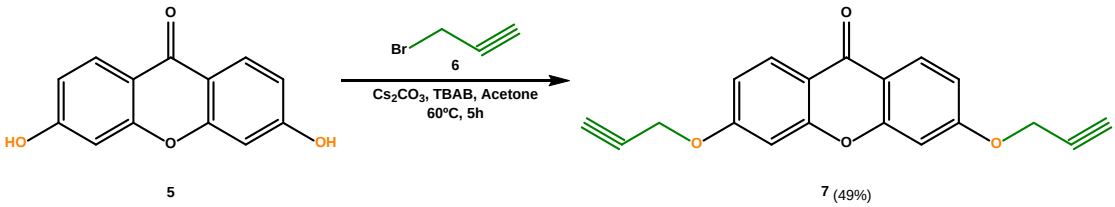

Scheme 5 - Synthesis of 3,6-bis(prop-2-yn-yloxy)-9*H*-xanthen-9-one (**7**).
TBAB:Tetrabutylammoniun bromide.

The bimolecular nucleophilic substitution (S_N2) involves the attack of a Lewis base or nucleophile to a Lewis acid or electrophile. In basic conditions, the phenol groups of 3,6-dihydroxy-9*H*-xanthen-9-one (**5**) are deprotonated and act as nucleophiles. Alkyl halides such as propargyl bromide (**6**) act as electrophiles since they have good leaving groups and are attacked by nucleophiles (**5**), suffering a halogen substitution (**Scheme 6**).

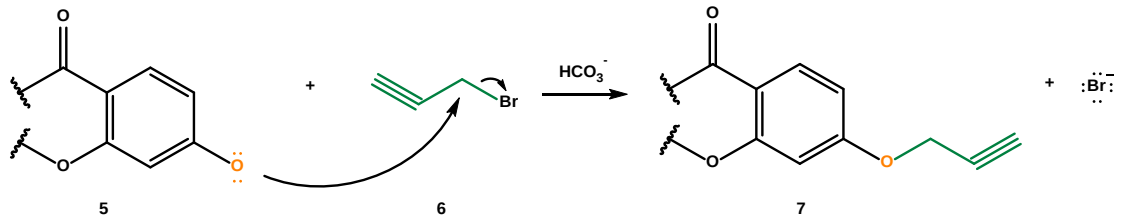

Scheme 6 - S_N2 Reaction mechanism to obtain 3,6-bis(prop-2-yn-yloxy)-9*H*-xanthen-9-one (**7**).

Acetone, an aprotic solvent, was selected since it will favour the reaction. Cesium carbonate is an inorganic base used to deprotonate phenolic groups of 3,6-dihydroxy-9*H*-xanthen-9-one (**5**). In this case, it is a catalyst promoting O-alkylation and it is not consumed during the reaction.

Since deprotonated compound **5** was not soluble in acetone, it was necessary to add tetrabutylammonium bromide (TBAB) to improve solubilisation [30].

2.1.4. 3,6-Bis(triazole ethyl 2,3,4,6-tetra-*O*-acetyl-*β*-D-*O*-glucopyranosyl)-9*H*-xanthen-9-one (9)

3,6-Bis(triazole ethyl 2,3,4,6-tetra-*O*-acetyl-*β*-D-*O*-glucopyranosyl)-9*H*-xanthen-9-one (**9**) was synthesized accordingly to the previous group experience by Cu(I)-catalysed azide-alkyne cycloaddition (CuAAC), using 2-azidoethyl 2,3,4,6-tetra-*O*-acetyl-*β*-D-glucopyranoside (**8**) and 3,6-bis(prop-2-yn-yloxy)-9*H*-xanthen-9-one (**7**) in the presence of $Cu_2SO_4 \cdot 5H_2O$ and sodium ascorbate, in a mixture of THF/H_2O (2:1), under MW irradiation, at 70ºC (**Scheme 7**).

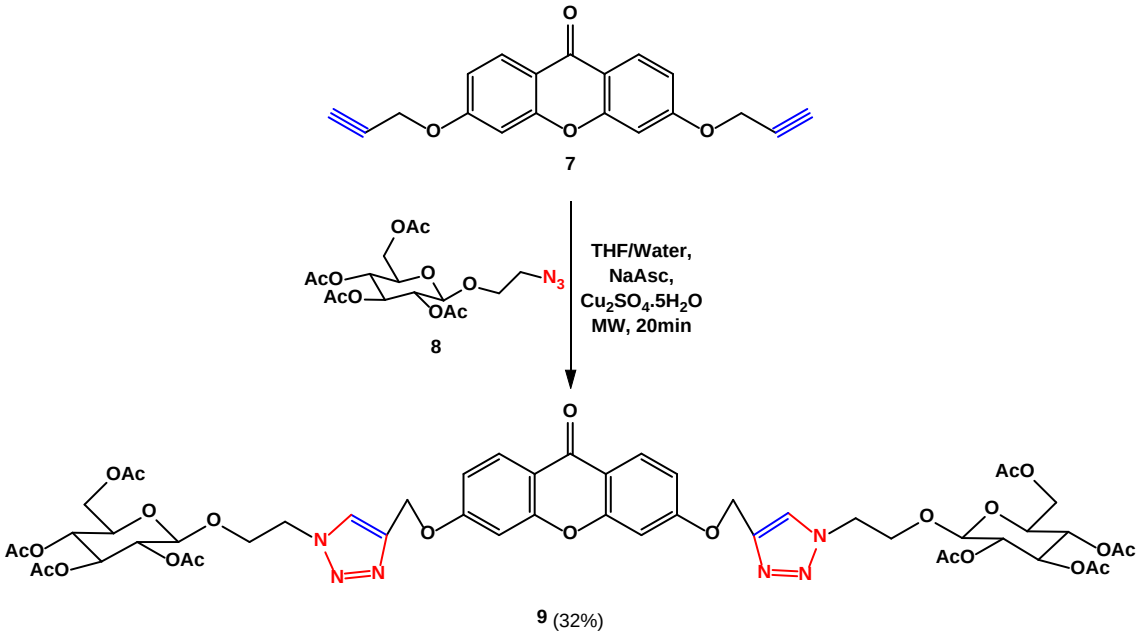

Scheme 7 - Synthesis of 3,6-bis(triazole ethyl 2,3,4,6-tetra-*O*-acetyl-*β*-D-*O*-glucopyranosyl)-9*H*-xanthen-9-one (**9**). THF: Tetrahydrofuran, NaAsc – Sodium ascorbate, MW -Microwave

The CuAAC reaction requires, at least, three components such as an azide, a terminal alkyne, and cooper (Cu) I catalyst. [31]. Cu (I) ions are prepared *in situ* by reduction of Cu (II) salts with a reduction agent such as sodium ascorbate, being more efficient, less costly and cleaner than Cu(I) salts [32].

One of the advantages of the CuAAC reaction is the possibility to perform it under an O_2 atmosphere. Cooper (I) does not react with water but reacts slowly with O_2 atmospheric to form copper oxide [31]. Although, since the reaction usually occurs in around half an hour there is no need for an inert atmosphere since the catalyst maintains its redox capacity. The catalyst is essential to complex with the terminal alkyne, forming a cooper (I) acetylide, and with azide ion (N_3^-) to ultimately form the triazole ring (**Scheme 8**) [32].

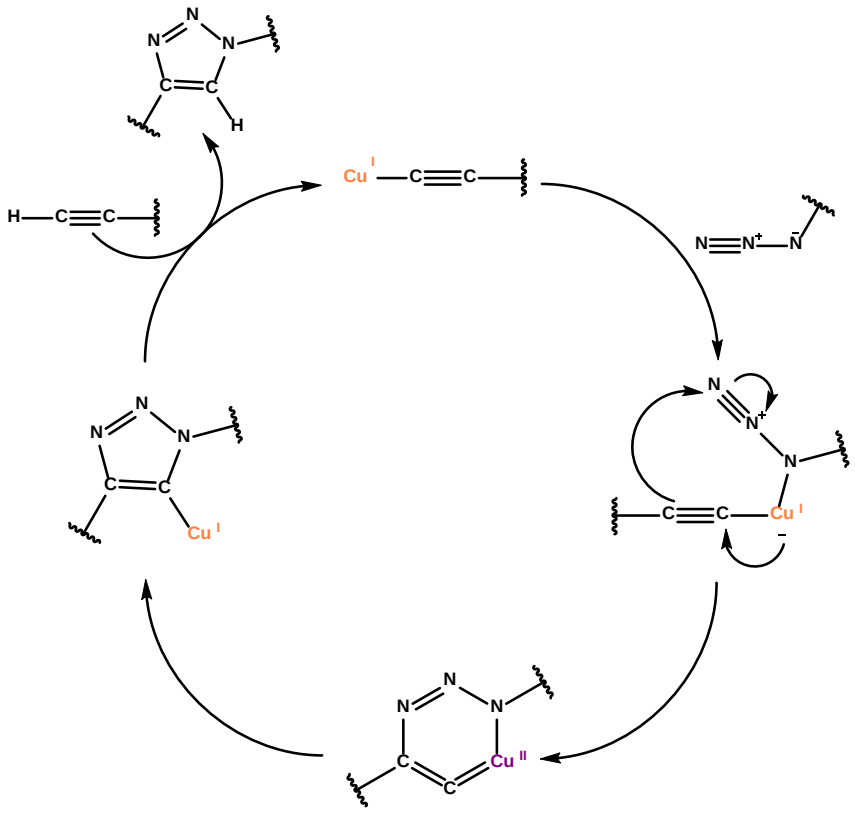

Scheme 8 - CuAAC reactional mechanism (adapted from [31]).

The use of MW irradiation allowed efficient internal heat transfer and, consequently, reduced reaction time (30 min) [32].

Purification of compound **9** was performed by liquid-liquid extraction with ethyl acetate, where the compound is soluble, and water to remove any inorganic compounds such as copper or sodium ascorbate. The solid obtained from the organic phase was purified by flash chromatography ($CHCl_3$:MeOH) to obtain the pure compound. However, the yield (32%) was lower than expected (36 %) due to the purification process.

2.1.5. 3,6-Bis(1-(1-(2,3,6,2',3',4',5'-hepta-*O*-acetyl-*β*-D-cellobiosyl)-1*H*-1,2,3-triazole-4-yl)methoxy)xanthone (11)

3,6-Bis(1-(1-(2,3,6,2',3',4',5'-hepta-*O*-acetyl-*β*-D-cellobiosyl)-1*H*-1,2,3-triazole-4-yl)methoxy)xanthone (**11**) was synthesized by a CuAAC reaction, using *β*-D-cellobiosyl azide heptaacetate (**10**) and 3,6-bis(prop-2-yn-yloxy)-9*H*-xanthen-9-one (**7**) in the presence of $Cu_2SO_4 \cdot 5H_2O$ and sodium ascorbate, in a mixture of THF/H_2O (2:1), under MW irradiation, at 70ºC (**Scheme 9**).

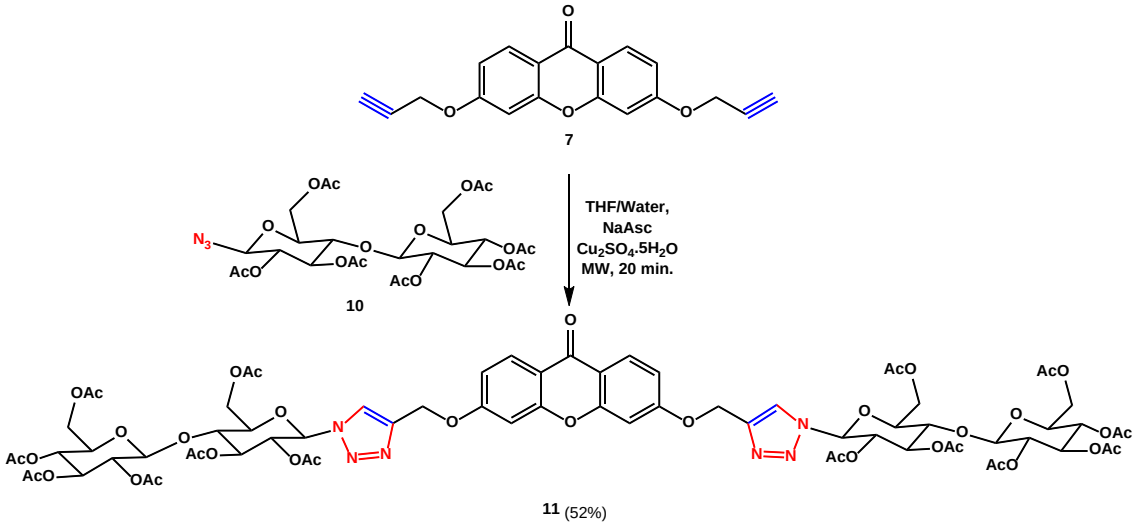

Scheme 9 - Synthesis of 3,6-bis(1-(1-(2,3,6,2',3',4',5'-hepta-*O*-acetyl-*β*-D-cellobiosyl)-1*H*-1,2,3-triazole-4-yl)methoxy)xanthone (**11**). THF:Tetrahydrofuran, NaAsc: Sodium ascorbate, MW: Microwave.

Purification of compound **11** was performed by liquid-liquid extraction with diclorometh ane, where the compound is soluble, and water to remove any inorganic compounds such as copper or sodium ascorbate. The solid obtained from the organic phase was crystallized with acetone to obtain the pure compound.

2.2. Structure elucidation

2.2.1. Gallic acid 3,5-disulfate (3)

The structure of gallic acid 3,5-disulfate (**3**, **Figure 9**) was established by Infrared (IR) and ^{1}H and ^{13}C Nuclear Magnetic Resonance (NMR).

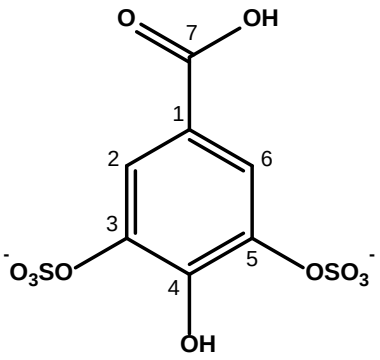

3

Figure 9 - Structure of gallic acid 3,5-disulfate (**3**).

The IR spectra of compound **3** (**Figure 10**) revealed important bands at 3526 cm^{-1} (OH phenolic), 1257 cm^{-1} (S=O) and 1071 cm^{-1} (C-O-S) confirming the success of sulfation of compound **1**.

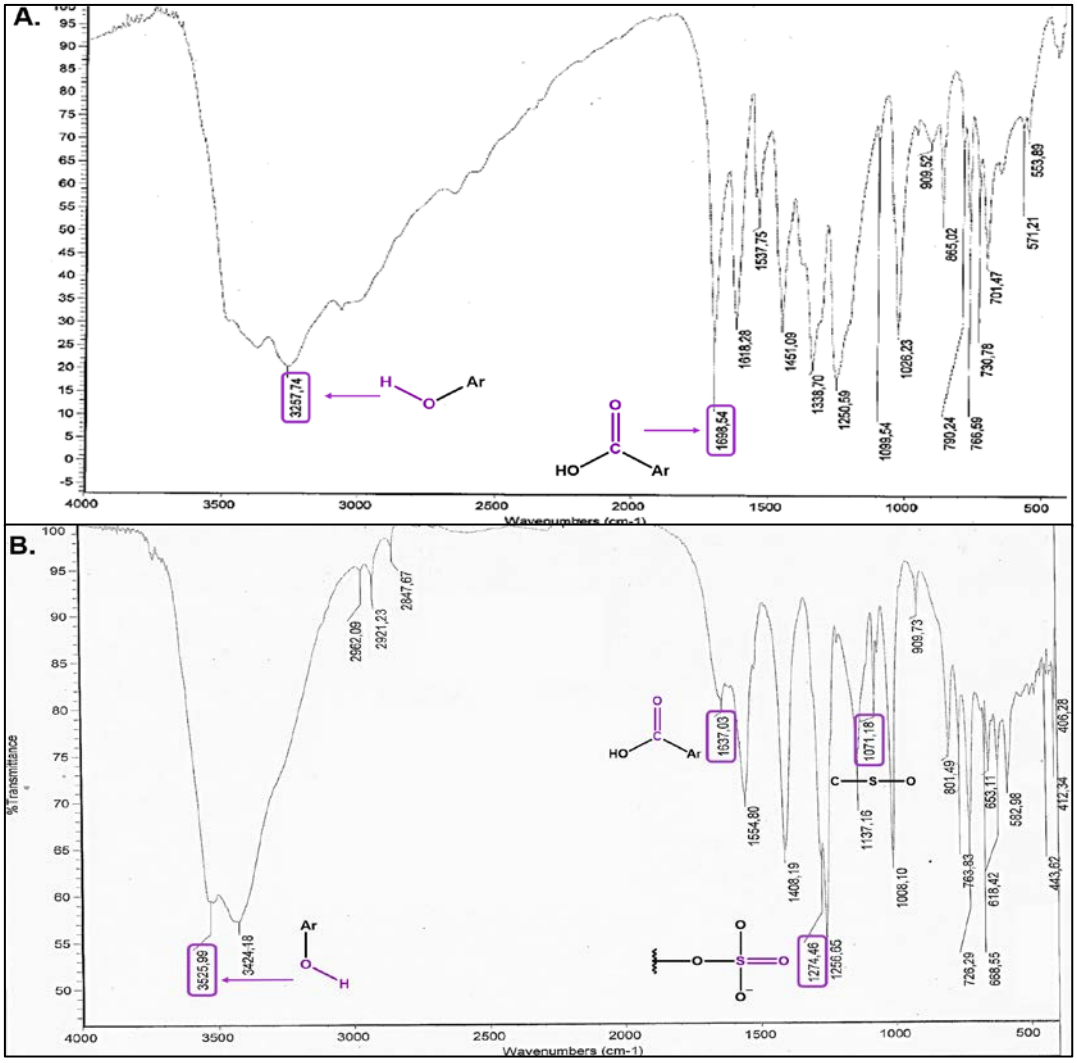

Figure 10 - IR spectra (KBr, cm^{-1}) of compounds **1** (A) and **3** (B).

The ^{1}H and ^{13}C NMR data of compounds **1** and **3** are represented in **Table 3**.

Table 3 - ^{1}H and ^{13}C NMR chemical shifts (δ) of compounds **1** and **3** (DMSO-d_6).

^{1}H	δ (ppm)		^{13}C	δ (ppm)	
	1	**3**		**1**	**3**
1	--	--		120.6	141.2
2	6.92 (s)	7.53 (s)		115.9	120.0
3	9.45 (brs)	--		145.5	169.0
4	9.45 (brs)	8.55 (s)		138.1	149.8
5	9.45 (brs)	--		145.5	169.0
6	6.92 (s)	7.53 (s)		115.9	120.0
7	--	--		167.7	174.5

The ^{1}H NMR spectra of compounds **1** and **3** is showed in **Figure 11**.

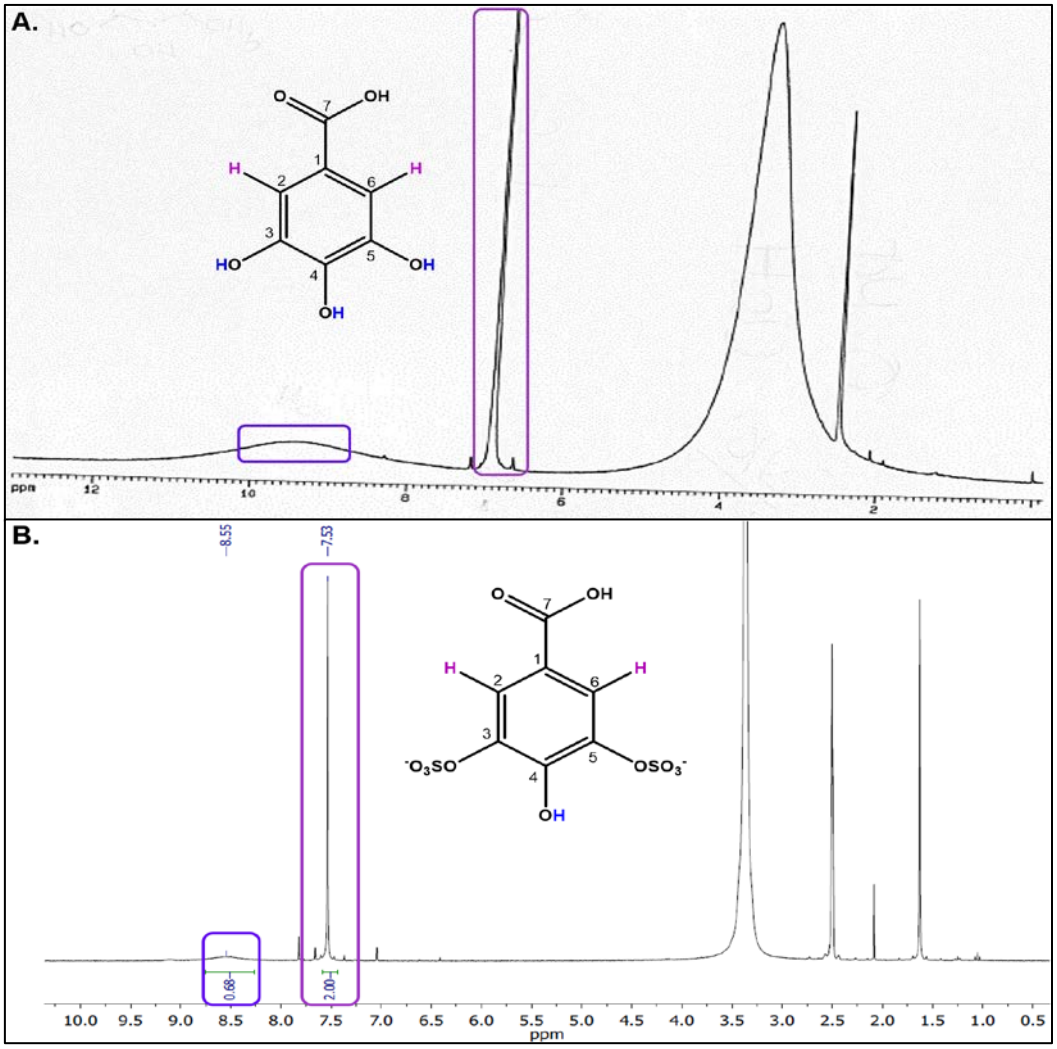

Figure 11 - ^{1}H NMR spectra (300.13 MHz, DMSO-d_6) of compound **1** (A) and **3** (B).

The ^{1}H NMR spectra of compound **3** showed deshielded aromatic protons, $C_{2/6}$ protons (δ_H 7.53) with reference to the same protons of compound **1** (δ_H 6.92). The signal at δ_H 8.55 correspond to the most acidic hydroxyl group (4-OH) that suffered desulfation during purification.

The ^{13}C NMR spectra of compounds **1** and **3** is showed in **Figure 12**.

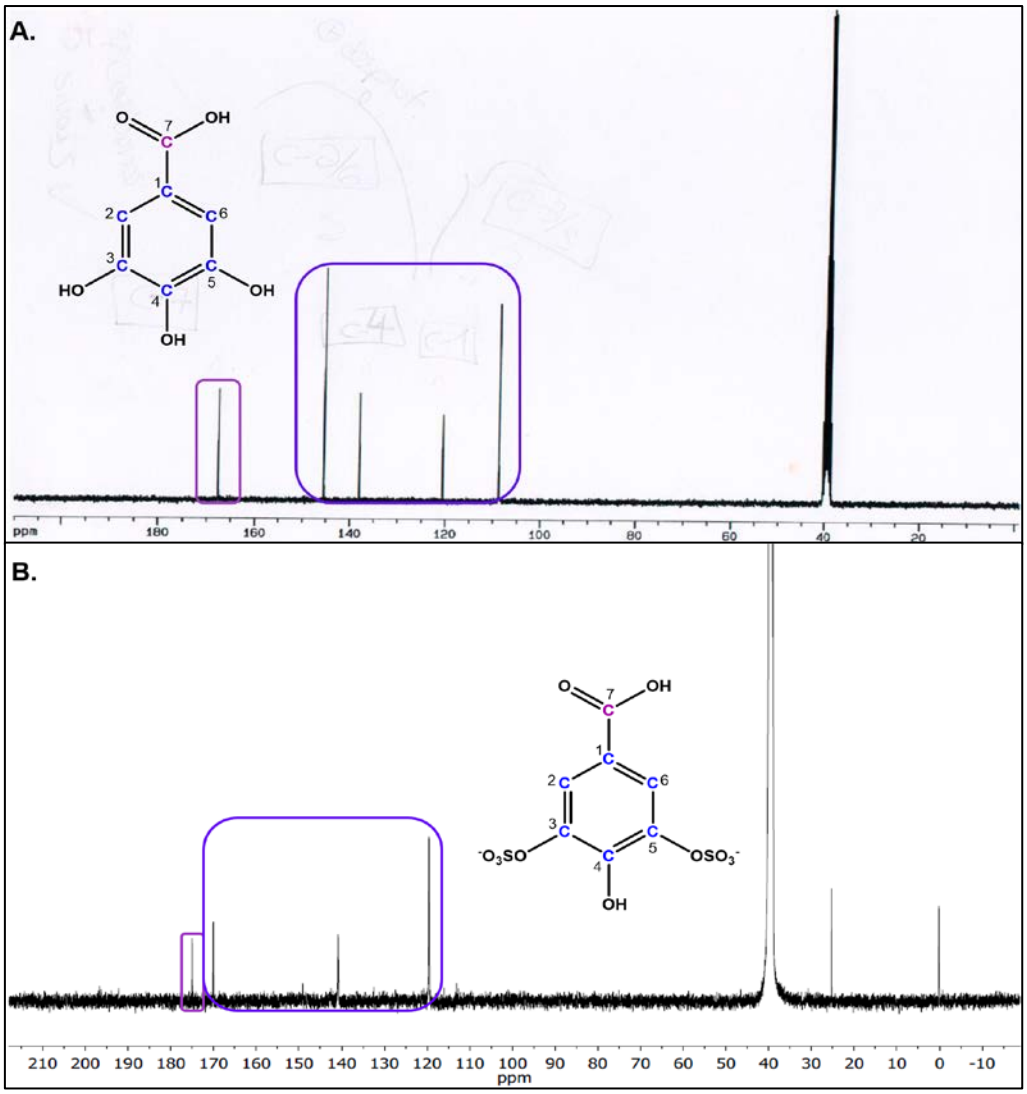

Figure 12 - ^{13}C NMR spectra (75.47MHz, DMSO-d_6) of compound **1** (A) and **3** (B).

The ^{13}C NMR spectra of compound **3** showed deshielded aromatic carbons, $C_{2/6}$ (δ_c 120.0) with reference to the same carbons of compound **1** (δ_c 115.9). Deshielded aromatic carbons $C_{3/5}$ (δ_c 174.5), were observed in compound **3** with reference to the same carbons of compound **1**, $C_{3/5}$ (δ_c 115.9).The carbon bonded to hydroxyl group, C_4 (δ_c 149.8), was deshielded due to the strong electron withdrawing sulfate groups and resonance effect with reference to the same carbon of compound **1**, C_4 (δ_c 138.1).

2.2.2. 3,6-Dihydroxy-9*H*-xanthen-9-one (5)

The structure of 3,6-dihydroxy-9*H*-xanthen-9-one (**5**, **Figure 13**) was established by IR and ^{1}H and ^{13}C NMR.

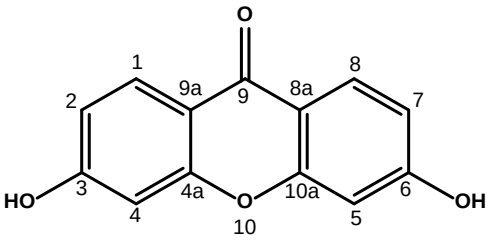

5

Figure 13 - Structure of 3,6-dihydroxy-9*H*-xanthen-9-one (**5**).

The IR spectra of compound **5** (**Figure 14**) revealed important bands at 3385 cm^{-1} (phenolic OH) and 1614 cm^{-1} (C=O).

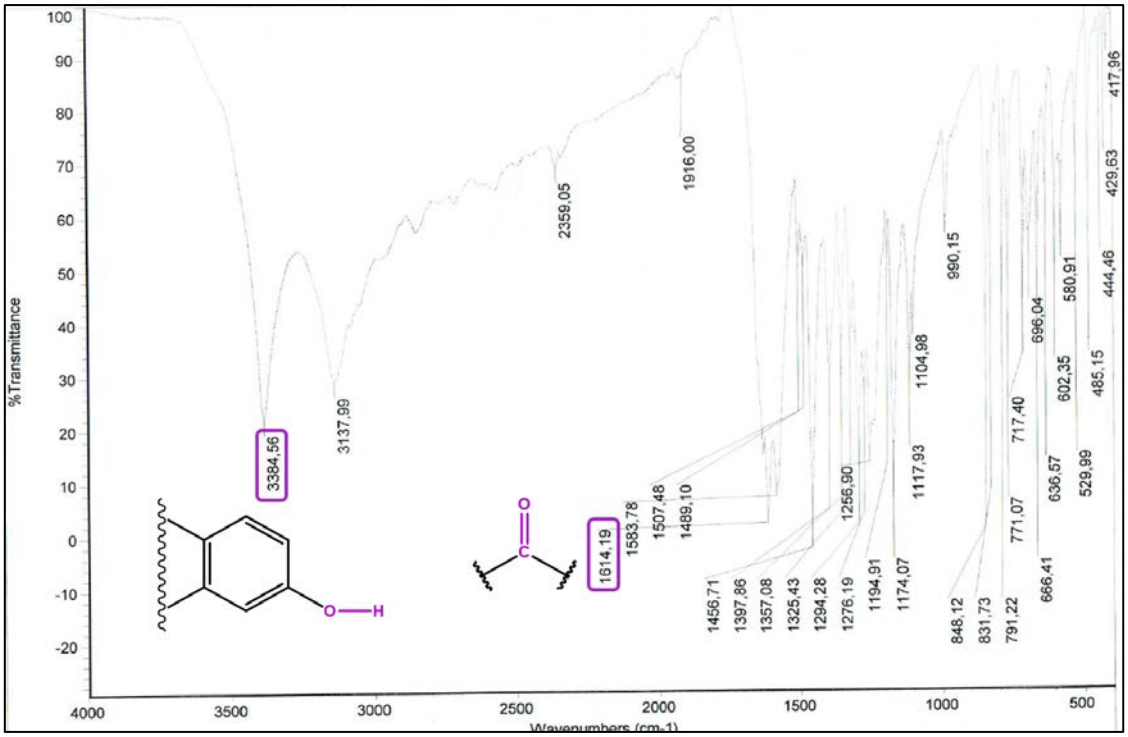

Figure 14 - IR spectra (KBr, cm^{-1}) of compound **5**.

The ^{1}H and ^{13}C NMR data of compounds **4** and **5** are represented in **Table 4**.

Table 4 - ^{1}H and ^{13}C NMR chemical shifts (δ) of compound **4** and **5** ($CDCl_3$).

^{1}H	δ (ppm)		^{13}C	δ (ppm)	
	4	**5**		**4**	**5**
1	--	8.00 (d, *J*= 8.7 Hz)		163.0	127.8
2	6.60 (s)	6.89 (dd, *J*= 2.1 and 8.7 Hz)		103.0	113.7
3	9.45 (s)	10.88 (s)		162.0	163.4
4	6.60 (s)	6.84 (d, *J*= 2.2 Hz)		114.0	102.1
4a	7.55 (s)	--		134.0	157.5
5	6.60 (s)	6.84 (d, *J*= 2.2 Hz)		114.0	102.1
6	9.45 (s)	10.88 (s, OH)		162.0	163.4
7	6.60 (s)	6.89 (dd, *J*= 2.1 and 8.7 Hz)		103.0	113.7
8	--	8.00 (d, *J*= 8.7 Hz)		163.0	127.8
8a	--	--		107.5	114.0
9	--	--		199.0	174.0
9a	--	--		107.5	114.0
10a	7.55 (s)	--		134.0	157.5

The ^{1}H NMR and ^{13}C NMR spectra of compound **5** are shown in **Figure 15**.

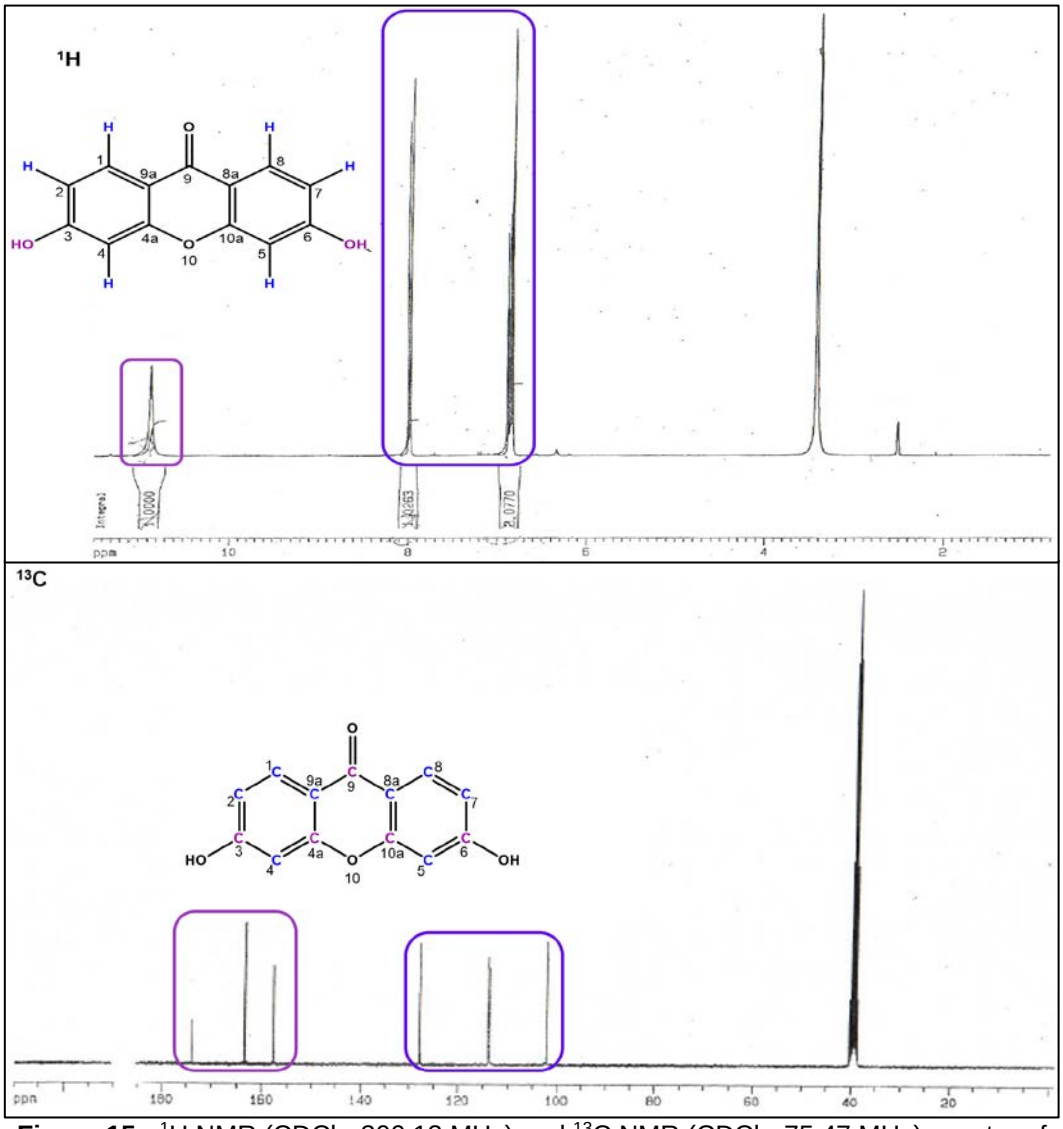

Figure 15 - ^{1}H NMR ($CDCl_3$, 300.13 MHz) and ^{13}C NMR ($CDCl_3$, 75.47 MHz) spectra of compound **5.**

The ^{1}H NMR spectra of compound **5** showed typical signals of the xanthone nucleus: a singlet (s) at δ_H 8.00 corresponding to H-1 and H-8; a double duplet (dd) at δ_H 6.89 corresponding to H-2 and H-7; and a duplet (d) at δ_H 6.84 corresponding to H-4 and H-5. The singlet (s) attributed to the hydroxyl groups (δ_H 10.88) reveals a withdrawing effect causing an increase in the chemical shift (deprotection).

The ^{13}C NMR spectra of compound **5** showed shielded aromatic carbons, $C_{1/8}$ (δ_c 127.8), $C_{9a/8a}$ (δ_c 114.0), $C_{2/7}$ (δ_c 113.7) and $C_{4/5}$ (δ_c 102.1). Deshielded aromatic carbon of xanthone carbonyl, C_9 (δ_c 174.0) and deshielded phenolic carbon, $C_{3/6}$ (δ_c 163.4) were observed in compound **5**.Deshielded aromatic

carbons connecting the two aromatic rings over an oxygen, $C_{4a/10a}$ (δ_C 157.5), were observed in compound **5**.

2.2.3. 3,6-Bis(prop-2-yn-yloxy)-9*H*-xanthen-9-one (7)

The structure of 3,6-bis(prop-2-yn-yloxy)-9*H*-xanthen-9-one (**7**, **Figure 16**) was established by IR and ^{1}H and ^{13}C NMR.

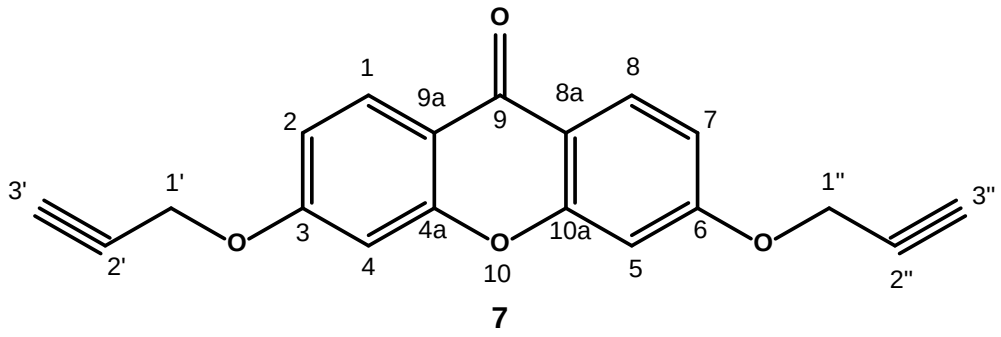

7

Figure 16 - Structure of 3,6-bis(prop-2-yn-yloxy)-9*H*-xanthen-9-one (**7**).

The IR spectra of compound **7** (**Figure 17**) revealed important bands at 2380 cm^{-1} (C≡C), 1613 cm^{-1} (C=O) and 1104 cm^{-1} (C-O ether) corresponding to the molecular modification performed.

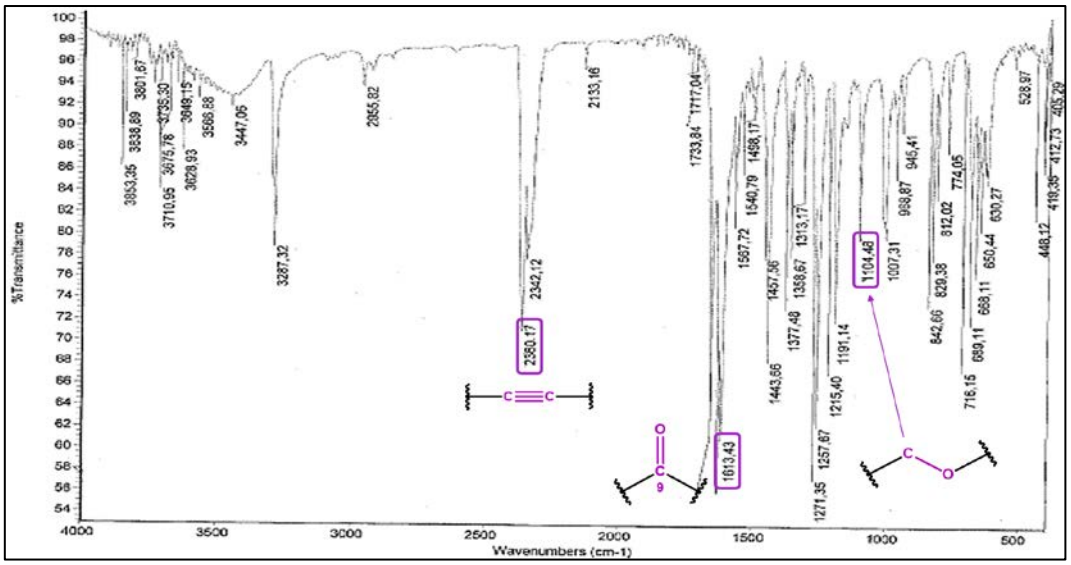

Figure 17 - IR spectra (KBr, cm^{-1}) of compound **7**.

The ^{1}H and ^{13}C NMR spectra of compound **7** are shown in **Figure 18**.

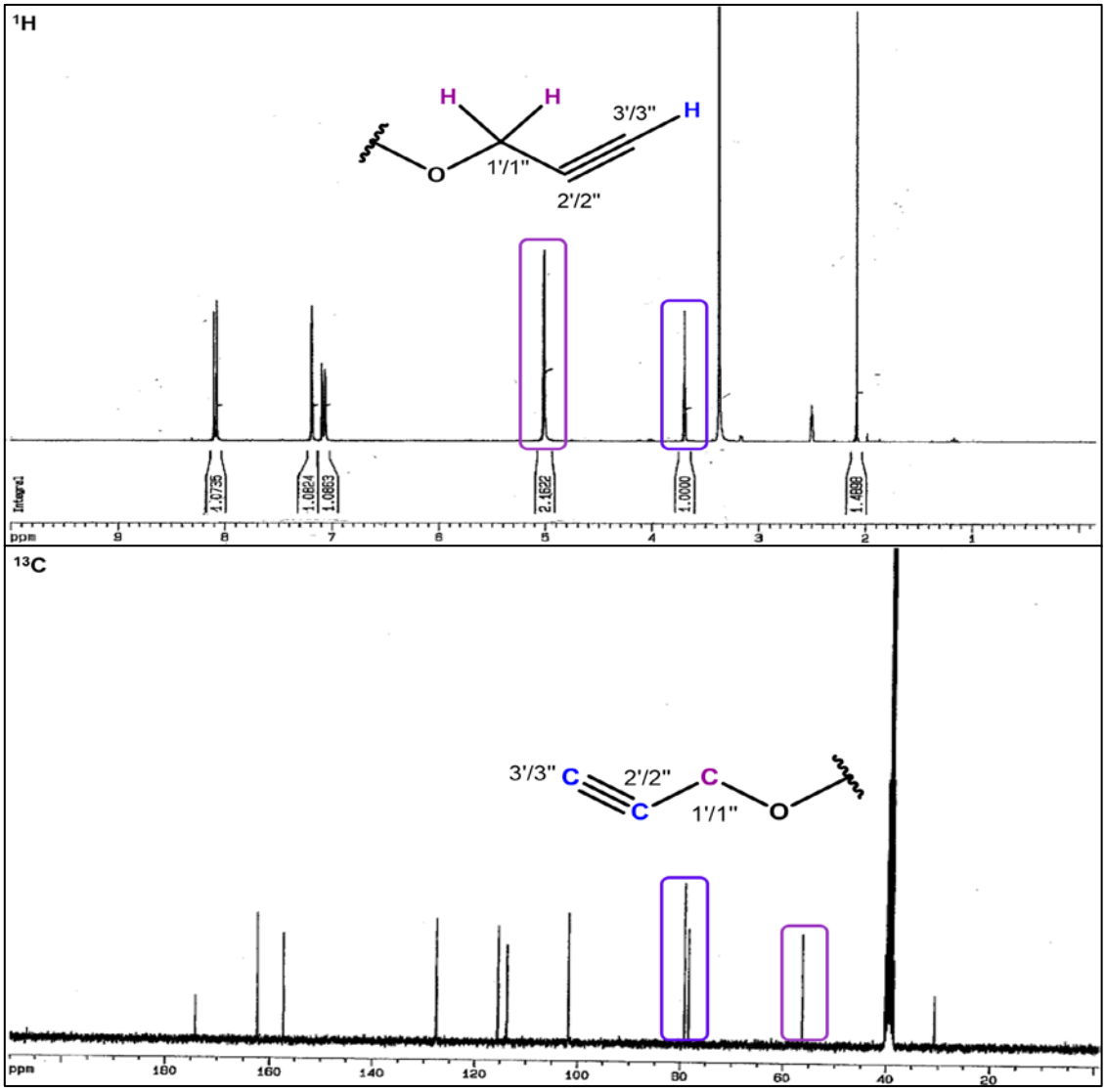

Figure 18 - ^{1}H ($CDCl_3$, 300.13 MHz) and ^{13}C ($CDCl_3$, 75.47 MHz) NMR spectra of compound **7**.

The ^{1}H NMR spectra of compound **7** showed typical signals of the xanthone nucleus. Two important signals at δ_H 5.01 (d, *J*=2.3 Hz) corresponding to protons $H_{1'}$ and $H_{1''}$, and δ 3.70 (t, *J*=2.3 Hz) corresponding to proton $H_{3'}$ and $H_{3''}$.

In the ^{13}C NMR spectra of compound **7** three signals appeared at δ_C 79.2 and δ_C 78.4 corresponding to $C_{2'}/C_{2''}$ and $C_{3'}/C_{3''}$, respectively; and at δ_C 56.3 from $C_{1'}/C_{1''}$ supporting the modifications performed on the xanthone nucleus.

2.2.4. 3,6-Bis(triazole ethyl 2,3,4,6-tetra-*O*-acetyl-*β*-D-*O*-glucopyranosyl)-9*H*-xanthen-9-one (9)

The structure of 3,6-bis(triazole ethyl 2,3,4,6-tetra-*O*-acetyl-*β*-D-*O*-glucopyranosyl)-9*H*-xanthen-9-one (**9**, **Figure 19**) was established by IR and ^{1}H and ^{13}C NMR.

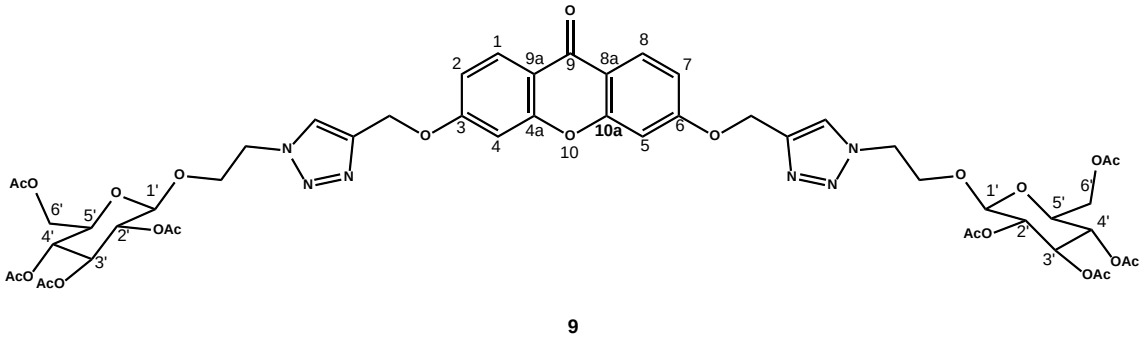

9

Figure 19 - Structure of 3,6-bis(triazole ethyl 2,3,4,6-tetra-*O*-acetyl-*β*-D-*O*-glucopyranosyl)-9*H*-xanthen-9-one (**9**).

The IR spectra of compound **9** (**Figure 20**) revealed the following important bands at 1754 cm^{-1} (C=O ester), 1608 cm^{-1} (C=C aromatic), 1227 cm^{-1} (C-O alkyl aryl ether) and 1106 cm^{-1} (C-O aliphatic ether).

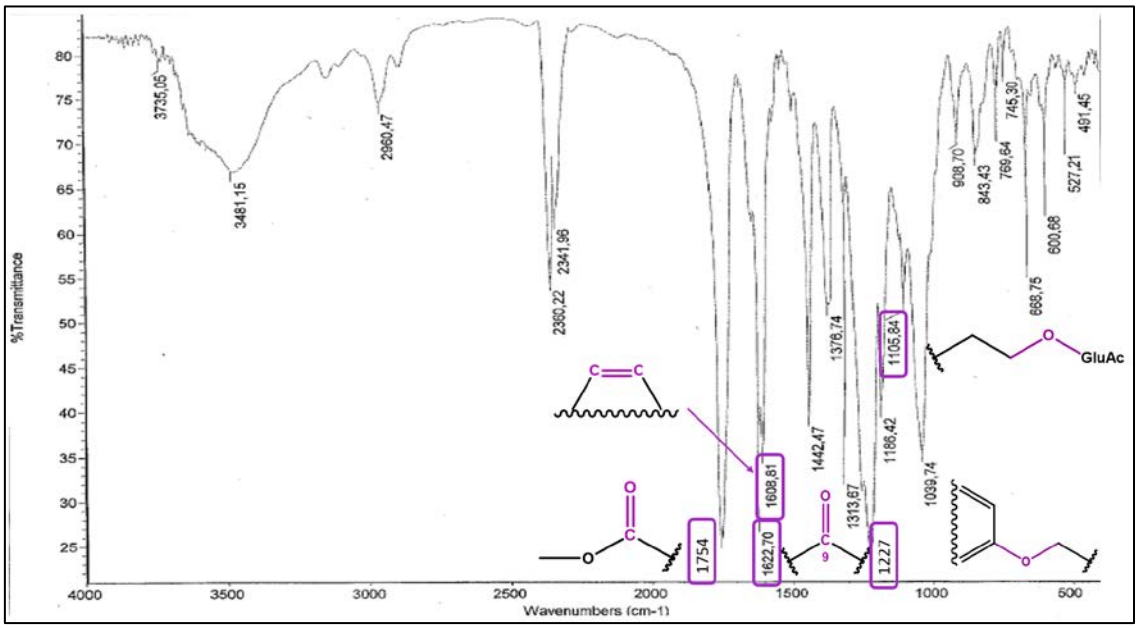

Figure 20 - IR spectra (KBr, cm^{-1}) of compound **9**.

The ^{1}H and ^{13}C NMR spectra of compound **9** are shown in **Figure 21**.

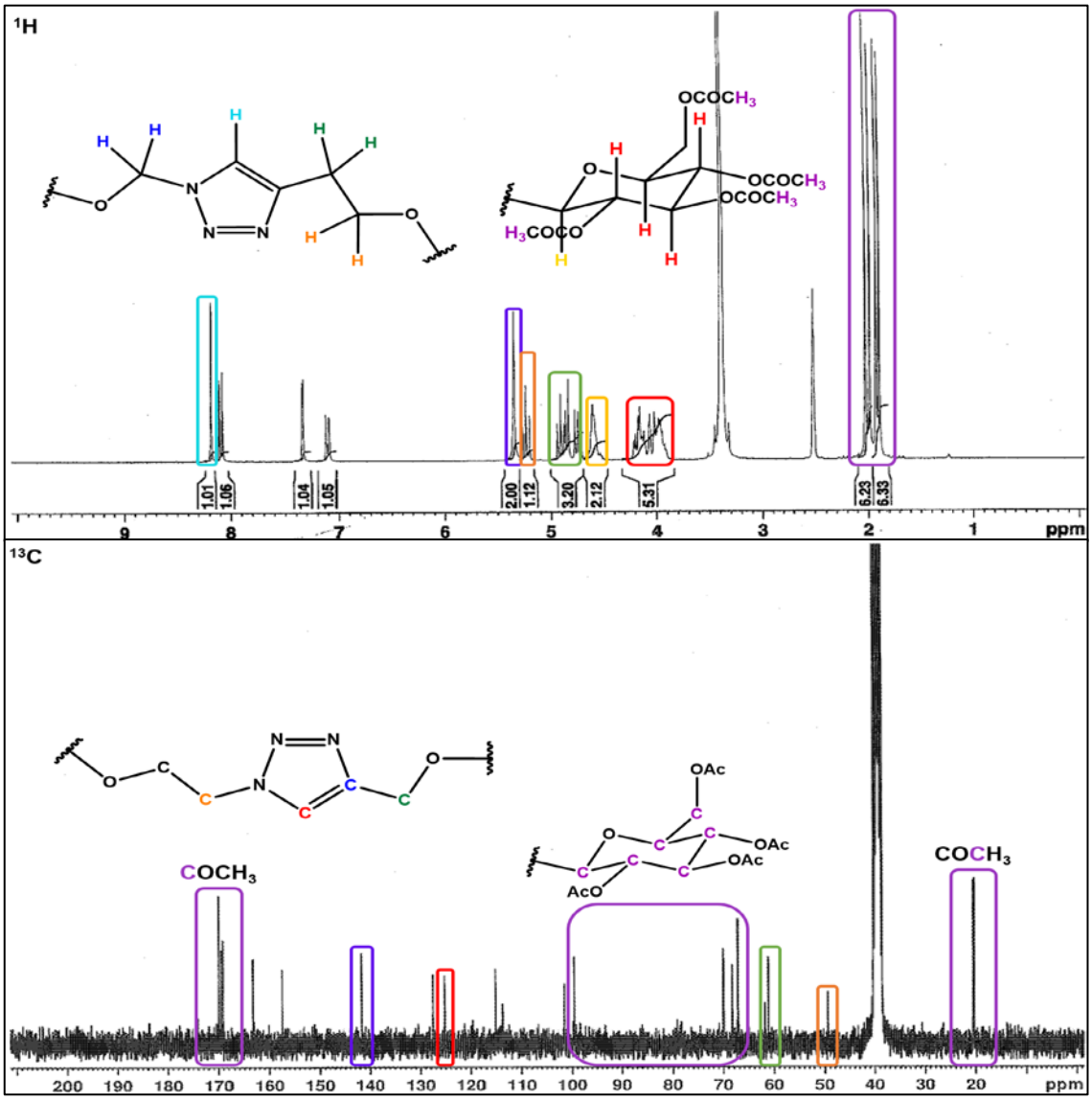

Figure 21 - ^{1}H ($CDCl_3$, 300.13 MHz) and ^{13}C ($CDCl_3$, 75.47 MHz) NMR spectra of compound **9**.

The ^{1}H NMR spectra of compound **9** revealed important signals that confirmed the success of the CuAAC reaction: a signal at δ_H 8.18 (s) attributed to the proton in the triazole ring; a signal at δ_H 5.34 (s) attributed to the two protons of the linker between the xanthone and the triazole ring; a triplet at δ_H 5.23 and a multiplet at δ_H 4.96-4.71 (m) attributed to the ethyl protons of the linker between the triazole ring and the acetoglucopyranosyl moiety; signals at δ_H 4.60-4.57 (m) and at δ_H 4.21-3.92 (m) were attributed to the glucose protons. Four singlets integrating for three protons each were observed between δ_H 2.02-1.89 and were attributed to the methyl protons of the four acetyl groups present in the acetoglucopyranosyl moiety.

The ^{13}C NMR spectrum also showed signals that confirmed the success of the CuAAC reaction: four signals between δ_C 170.1-169.0 attributed to the four carbonyl groups of the acetyl groups of the acetoglucopyranosyl; signals at δ_C 141.7 (N-CH=*C*- triazole) and δ_C 125.2 (N-*C*H=C triazole) attributed to the carbons present in the triazole ring; six signals between δ_C 86.4-61.9 attributed to the glucose carbons; and four signals between δ_C 20.5-20.2 attributed to the methyl carbons of the acetyl groups of acetoglucopyranosyl moiety.

2.2.5. 3,6-Bis(1-(1-(2,3,6,2',3',4',5'-hepta-*O*-acetyl-*β*-D-cellobiosyl)-1*H*-1,2,3-triazole-4-yl)methoxy)xanthone (11)

The structure of 3,6-bis(1-(1-(2,3,6,2',3',4',5'-hepta-*O*-acetyl-*β*-D-cellobiosyl)-1*H*-1,2,3-triazole-4-yl)methoxy)xanthone (**11**, **Figure 22**) was established by IR and ^{1}H and ^{13}C NMR.

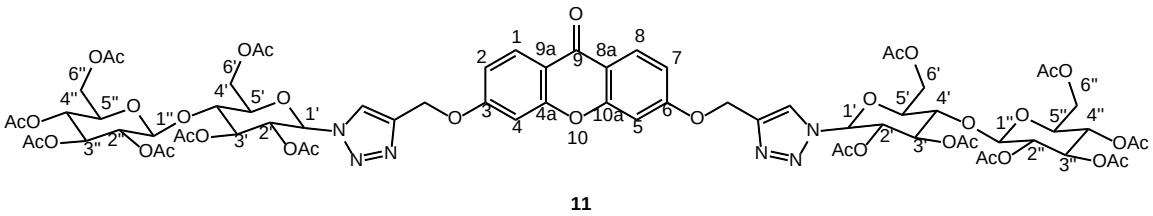

11

Figure 22 - Structure of 3,6-bis(1-(1-(2,3,6,2',3',4',5'-hepta-*O*-acetyl-*β*-D -cellobiosyl)-1*H*-1,2,3-triazole-4-yl)methoxy)xanthone (**11**).

The IR spectra of compound **11** (**Figure 23**) revealed the following important bands at 1754 cm^{-1} (C=O ester), 1611 cm^{-1} (C=C aromatic), 1230 cm^{-1} (C-O-C alkyl aryl ether), 1102 cm^{-1} (C-O ether) and 1041 cm^{-1} (C-O ether cellobiose).

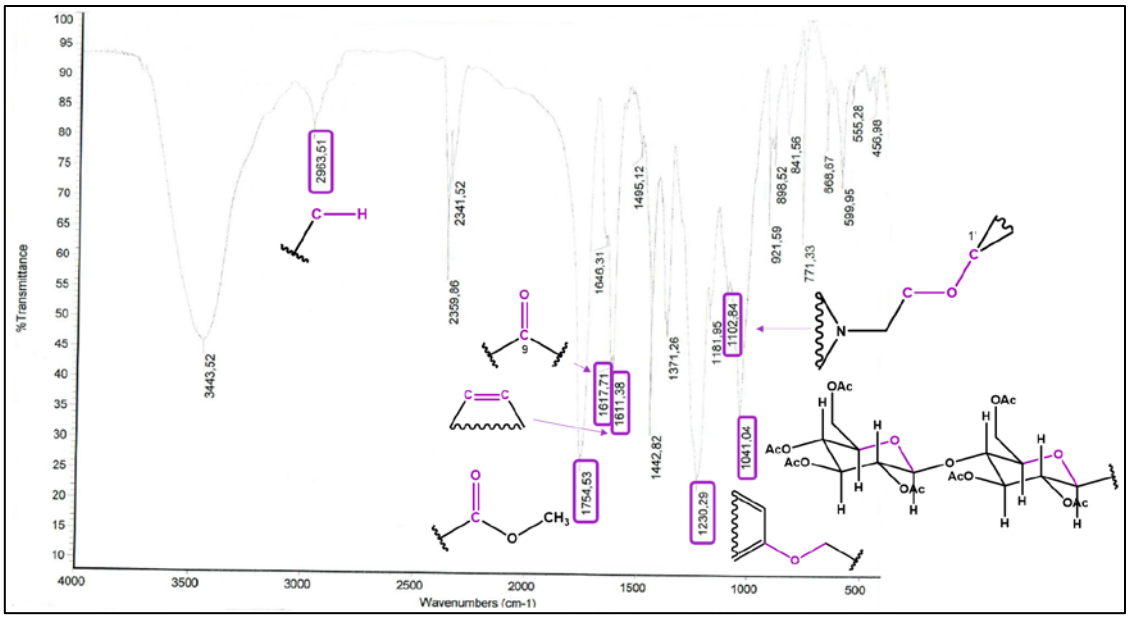

Figure 23 - IR spectra (KBr, cm^{-1}) of compound **11**.

The ^{1}H and ^{13}C NMR spectra of compound **11** are shown in **Figure 25**. The signals concerning cellobiose were attributed using two-dimensional nuclear magnetic resonance spectroscopy such as correlation spectroscopy (^{1}H-^{1}H COSY) (**Figure 24**).

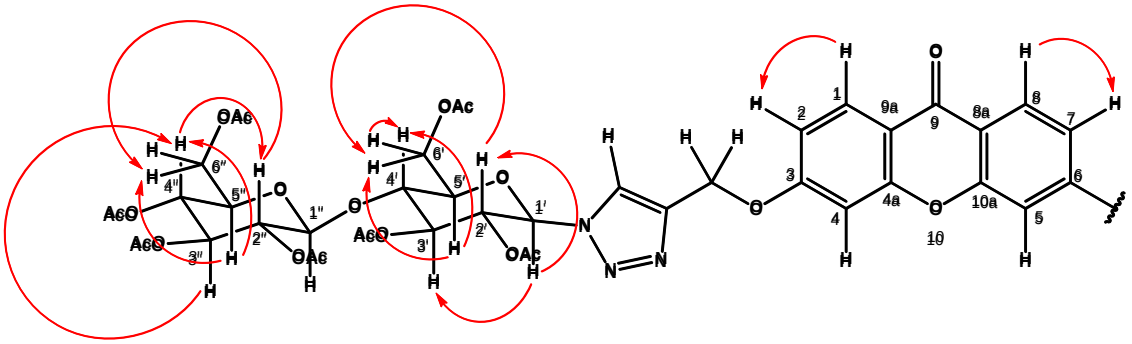

Figure 24 - COSY correlations of compound **11**.

The ^{1}H NMR spectra of compound **11** revealed important signals that confirmed the success of the CuAAC reaction: a singlet at δ_H 7.85 attributed to the proton of the triazole ring; a singlet at δ_H 5.32 attributed to the two protons of the linker between the xanthone and the triazole ring; signals at δ_H 5.86-3.66 were attributed to the cellobiose protons. Four signals integrating for twenty one protons each were observed between δ_H 2.16-1.83 and were attributed to the methyl of the acetyl groups present in the acetocellobiose moiety.

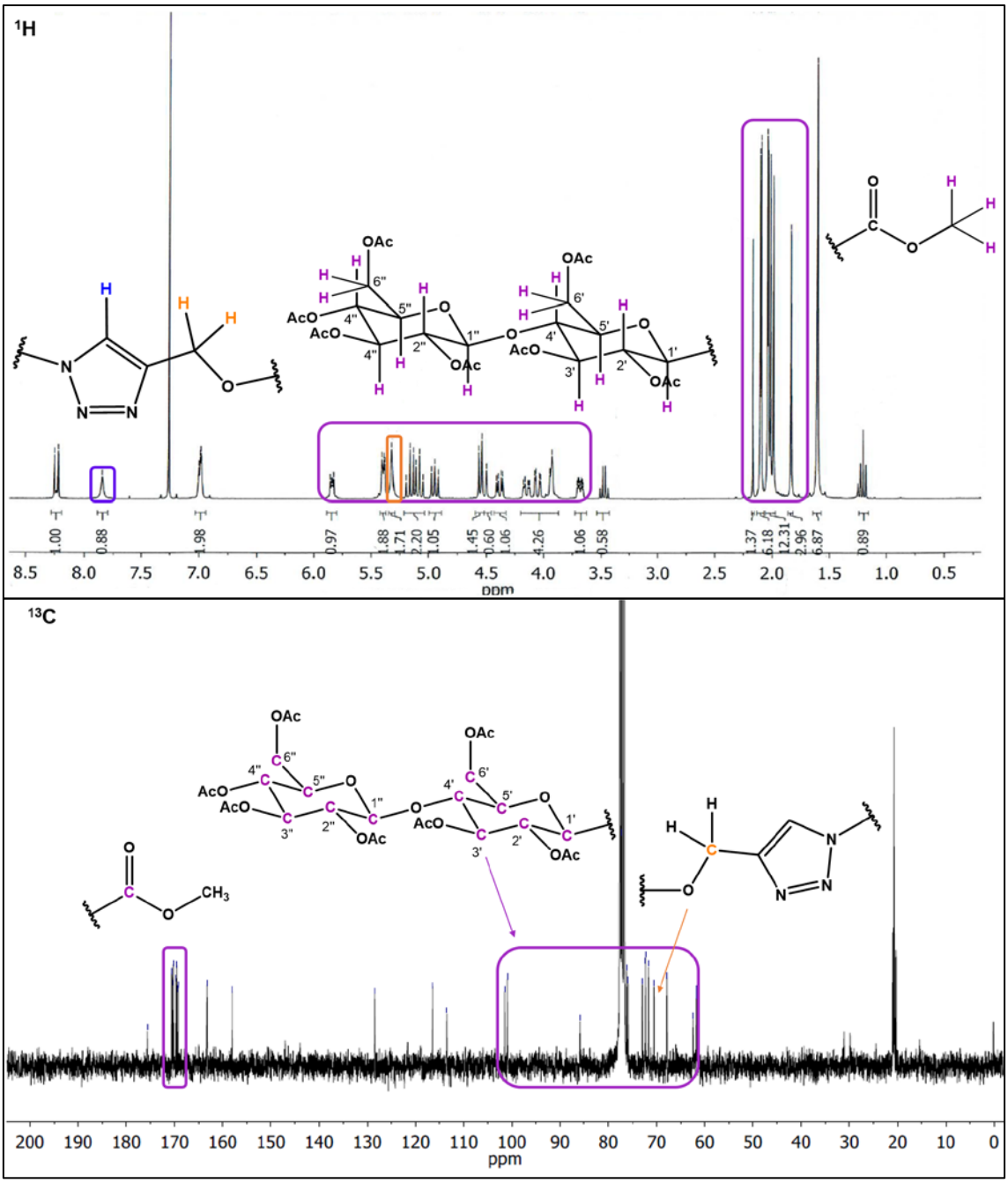

Figure 25 - ^{1}H ($CDCl_3$, 300.13 MHz) and ^{13}C ($CDCl_3$, 75.47 MHz) NMR spectra of compound **11**.

The ^{13}C NMR spectra also showed signals that confirmed the success of the CuAAC reaction: seven signals between δ_C 170.6-169.2 were attributed to the carbonyl carbons of the acetyl groups of the acetocellobiose; signals between δ_C 101.5-61.7 were attributed to the cellobiose carbons; and a signal at δ_C 75.9 was attributed to the two carbons of the linker between the xanthone and the triazole ring.

3. EXPERIMENTAL

3.1. General methods and materials

Commercial available reagents were purchased from Sigma-Aldrich, TCI and Synthose. Solvents were evaporated using rotary evaporated under reduced pressure (Buchi Waterchath B-480). Microwave reactions were performed in reaction vessels, opened or closed, usig a MicroSYNTH 1600 synthesizer from Milestone (ThermoUnicam, Portugal). Reactions were monitored by TLC carried out in plates of silica gel (60 F254 Merck). Compounds were visually detected by absorbance at 254 and/or 365 nm, H_2SO_4 in 20% MeOH followed by heat activation or $FeCl_3$ 10% MeOH solution. Purification of compounds was performed either by flash chromatography using Fluka silica gel 60 (0.04 – 0.063 nm) and/or by crystallization. IR spectra were measured on an ATI Mattson Genesis series FTIR spectrophotometer, in KBr microplates (cm^{-1}). ^{1}H and ^{13}C NMR spectra were performed in the Department of Chemistry of the University of Aveiro and were taken in DMSO-d_6 or $CDCl_3$ at room temperature on Bruker Avance 300 instruments (300.13 for ^{1}H and 75.47 MHz for ^{13}C). Chemical shifts are expressed as δ (ppm) values relative to tetramethysilane as an internal reference. Coupling constants (*J*) are reported in hertz (Hz). Assignment abbreviations are the following: singlet (s), doublet (d), triplet (t), multiplet (m), and doublet of doublets (dd).

3.2. Synthesis

3.2.1. Synthesis of gallic acid 3,5-disulfate (3)

To a solution of gallic acid (0.2 g, 1.17 mmol) in DMA (4 mL), TEA·SO_3 (3 eq/OH; 1.92 g, 10.6 mmol) was added. The mixture was kept under MW irradiation (400 W), in a closed vessel, at 100 °C, for 5h30min. This procedure was performed in nine parallel closed vessels. The reactions were controlled by TLC using $CHCl_3$:MeOH:HCOOH (7:3:0.1) as mobile phase. After cooling to room temperature, the nine reaction mixtures were transferred to nine flasks with acetone (100-150 mL). To every flask, triethylamine was added until the formation of a dark brown oil. The supernatant was removed by decantation and the oils were joined, after washing with acetone and ether. A sodium acetate solution 30 % (250 mL) was added until solubilized the oil. The solid formed with the addition of sodium acetate was removed by filtration and washed with cold ethanol. The

filtrate was concentrated under reduced pressure, and sodium acetate solution 30 % was added to the crude oil. The solid formed after adding ethanol was filtrated under vacuum and washed with cold ethanol (2.25g, 45% yield, MP 280ºC (ethanol)). IR (KBr): 3526 (O-H phenolic), 2962 (O-H carboxylic acid), 1637 (C=O carboxylic acid), 1554 (C=C aromatic), 1257 (S=O), 1071 (C-O-S), 910 (C-H aromatic) cm^{-1}. ^{1}H NMR (DMSO-d_6, 300.13 MHz) δ: 8.55 (1H, s, OH-4), 7.53 (2H, s, H-2/H-6) ppm. ^{13}C NMR (DMSO-d_6, 75.47 MHz) δ: 174.5 (C-7), 169.0 (C-3/C-5), 149.8 (C-4), 141.2 (C-1), 120.0 (C-2/C-6) ppm.

3.2.2. Synthesis of 3,6-dihydroxy-9*H*-xanthen-9-one (5)

To a porcelain capsule 2,2',4,4'-tetrahidroxy-benzophenone (0.5 g, 2.03 mmol) was added and placed in the furnace, at 220ºC, for 1 hour. The reaction was controlled by TLC using n-hexane:ethyl acetate (6:4) as mobile phase. 3,6-dihydroxy-9*H*-xanthen-9-one was obtained as a brown solid (0.36 g, 78% yield, MP > 350ºC). IR (KBr): 3385 (phenolic OH), 1614 (C=O ketone), 1584 (C=C aromatic), 1507 (C=C aromatic) cm^{-1}. ^{1}H NMR ($CDCl_3$, 300.13MHz) δ: 10.88 (1H, s, OH), 8.00 (1H, d, *J*=8.7 Hz, H-1/H-8), 6.89 (1H, dd, *J*= 2.1 and *J*= 8.7 Hz, H-2/H-7), 6.84 (1H, d, *J*=2.2 Hz, H-4/H-5) ppm. ^{13}C NMR ($CDCl_3$, 75.47 MHz) δ: 174.0 (C-9), 163.4 (C-3/C-6), 157.5 (C-4a/C-10a), 127.8 (C-1/C-8), 114.0 (C-8a/C-9a), 113.7 (C-2/C-7), 102.1 (C-4/C-5) ppm.

3.2.3. Synthesis of 3,6-bis(prop-2-yn-yloxy)-9*H*-xanthen-9-one (7)

To a solution of 3,6-dihydroxy-9*H*-xanthen-9-one (2.0 g, 8.76 mmol), $CsCO_3$ (11.8 g, 36.2 mmol) and TBAB (11.1 g, 34.4 mmol) in anhydrous acetone (50 mL), a solution of propargyl bromide 80% in toluene (15.1 g, 126.7 mmol) was added under anhydrous conditions. The mixture was refluxed at 60ºC, for 5 hours. The reaction was controlled by TLC using $CHCl_3$:MeOH:HCOOH (95:5:0.1) as mobile phase and sprayed with a solution of ferric chloride. The reaction was cooled to room temperature, vacuum filtered and dried under reduced pressure obtaining a brown oil. The brown oil was then dissolved in dichloromethane and extracted twice with a solution of NaOH 5%. The organic phase was washed with water and the aqueous phase with diclorometane. The combined organic phases were dried over anhydrous sodium sulfate, filtered and concentrated under reduced pressure. The concentrated organic phase was

purified by crystallization with methanol to obtain 3,6-bis(prop-2-yn-yloxy)-9*H*-xanthen-9-one as an orange solid (1.3 g, 49 % yield, MP 188-190ºC (methanol)). IR (KBr) cm^{-1}: 2956 (C-H aliphatic), 2133 (C≡C), 1613 (C=O ketone), 1568 (C=C aromatic), 1541 (C=C aromatic), 1104 (C-O ether). ^{1}H NMR ($CDCl_3$, 300.13 MHz) δ: 8.09 (2H, d, *J*=8.9 Hz, H-1/H-8), 7.19 (1H, d, *J*=2.4 Hz, H-4/H-5), 7.08 (1H, dd, *J*=2.44, *J*=8.8 Hz, H-2/H-7), 5.01 (2H, d, *J*=2.3 Hz, H-1'/H-1''), 3.70 (1H, t, *J*=2.3 Hz, H-triple) ppm. ^{13}C NMR ($CDCl_3$, 75.47 MHz) δ: 174.1 (C-9), 162.4 (C-3/C-6), 157.2 (C-4a/C-10a), 127.6 (C-1/C-8), 115.5 (C-8a/C-9a), 113.8 (C-2/C-7), 101.8 (C-4/C-5), 79.2 (C-2'), 79.4 (C-3'), 56.3 (C-1') ppm.

3.2.4. Synthesis of 3,6-bis(triazole ethyl 2,3,4,6-tetra-*O*-acetyl-*β*-D-*O*-glucopyranosyl)-9*H*-xanthen-9-one (9)

To a solution of 3,6-bis(prop-2-yn-yloxy)xanthone (0.18 g, 0.6 mmol) and 2-azidoethyl 2,3,4,6-tetra-*O*-*β*-D-glucopyranoside (0.5 g, 1.2 mmol) in THF (20 mL), a solution of sodium ascorbate (0.47 g, 2.4 mmol) and $Cu_2SO_4 \cdot 5H_2O$ (0.3 g, 1.2 mmol) in water (10 mL) was added. The mixture was kept under MW irradiation (200W), in a closed vessel, at 70 °C, for 20 minutes. The reaction was controlled by TLC using $CHCl_3$:MeOH (95:5) as mobile phase. The reaction was cooled to room temperature, vacuum filtered and concentrated under reduced pressure in water. The water suspension was then extracted twice with ethyl acetate and the organic phase was washed with water. The combined organic phases were dried over anhydrous sodium sulfate, filtered and concentrated under reduced pressure. The concentrated organic phase was purified by flash chromatography (SiO_2; $CHCl_3$:MeOH) to obtain 3,6-bis(triazole ethyl 2,3,4,6-tetra-*O*-acetyl-*β*-D-*O*-glucopyranosyl)-9*H*-xanthen-9-one as a white solid (0.23 g, 32 % yield, MP 155-190ºC (chloroform and methanol)). IR (KBr) cm^{-1}: 2960 (C-H aliphatic), 1754 (C=O ester), 1622 (C=O ketone) 1608 (C=C aromatic), 1442 (C-H aliphatic), 1376 (C-H aliphatic), 1227 (C-O alkyl aryl ether), 1106 (C-O aliphatic ether) cm^{-1}. ^{1}H NMR ($CDCl_3$, 300.13 MHz) δ: 8.18 (1H,s, triazole *H*), 8.09 (2H, d, *J*=8.9 Hz, H-1/H-8), 7.34 (2H, d, *J*=2.2 Hz, H-4/H-5), 7.10 (2H, dd, *J*=2.25, *J*=8.9 Hz, H-2/H-7), 5.34 (2H, s, OCH_2-triazole), 5.23 (1H, t, *J*=9.5 Hz, triazole-CH_2CH_2O-Glu), 4.94-4.71 (3H, m, triazole-CH_2CH_2O-Glu), 4.60-4.57 (2H, m, H-Glucose), 4.21-3.92 (5H, m, H-Glucose), 2.02 (3H, s, -COCH_3), 1.98 (3H, s, -COCH_3), 1.92 (3H, s, -COCH_3), 1.89 (3H, s, -COCH_3) ppm.^{13}C NMR ($CDCl_3$,

75.47 MHz) δ: 174.1 (C-9), 170.1 (*C*OCH$_3$), 169.6 (*C*OCH$_3$), 169.3 (*C*OCH$_3$), 169.0 (*C*OCH$_3$), 163.3 (C-3/C-6), 157.4 (C-4a/C-10a), 141.7 (CH=*C* triazole), 127.6 (C-1/C-8), 125.2 (*C*H=C triazole), 115.2 (C-8a/C-9a), 113.9 (C-2/C-7), 101.5 (C-4/C-5), 86.4 (C-1'), 71.9 (C-5'), 70.7 (C-3'), 68.06 (C-2'), 67.4 (C-4'), 61.9 (C-6'), 61.2 (O-*C*H$_2$), 49.4 (*C*H$_2$-N), 20.5 (CO*C*H$_3$), 20.4 (CO*C*H$_3$), 20.2 (2 CO*C*H$_3$) ppm.

3.2.5. Synthesis of 3,6-bis(1-(1-(2,3,6,2',3',4',5'-hepta-*O*-acetyl-*β*-D-cellobiosyl)-1*H*-1,2,3-triazole-4-yl)methoxy)xanthone (11)

To a solution of 3,6-bis(prop-2-yn-yloxy)xanthone (0.3 g, 0.99 mmol) and celobiosyl-heptacetate (2 g, 3.02 mmol) in THF (10 mL), a solution of sodium ascorbate (0.78 g, 3.9 mmol) and $Cu_2SO_4 \cdot 5H_2O$ (0.49 g , 1.97 mmol) in water (7 mL) was added. The mixture was kept under MW irradiation (200W), in an open vessel, at 70 °C, for 20 minutes, obtaining a brown gel. The reaction was controlled by TLC using $CHCl_3$:MeOH:HCOOH (95:5:0.1) and $CHCl_3$:MeOH:HCOOH (7:3:0.1) as mobile phases. The reaction was cooled to room temperature, vacuum filtered with dichloromethane and concentrated under reduced pressure. Then filtrated was extracted twice and washed with water. The combined organic phases were dried over anhydrous sodium sulfate, filtered and concentrated under reduced pressure. The concentrated organic phase was purified by crystallization with acetone to obtain 3,6-bis(1-(1-(2,3,6,2',3',4',5'-hepta-*O*-acetyl-β-D-cellobiosyl)-1*H*-1,2,3-triazole-4-yl)methoxy)xanthone as a white solid (0.44 g, 52 % yield, MP 268-269ºC (acetone)). IR (KBr): 2963 (-C-H alkane), 1754 (C=O acetyl), 1617 (C=O), 1611 (C=C triazole), 1442 (C-H methyl), 1230 (C-O-C alkyl aryl ether), 1102 (C-O ether), 1041 (C-O ether celobiose) cm^{-1}. ^{1}H NMR ($CDCl_3$, 300.13MHz) δ: 8.24 (1H, d, *J*=9.4, H-1/H-8), 7.85 (1H, s, *H*-triazole), 7.01-6.98 (2H, m, H-2/H-4/H-5/H-7), 5.86-5.83 (1H, m, H-1'), 5.41-5.38 (2H, m, H-2'/H-3'), 5.32 (2H, s, O-C*H$_2$*-triazole), 5.19-5.05 (2H, m, H-1''/H-3''), 4.97-4.92 (1H, t, *J*=9 Hz, H-4''), 4.57-4.54 (1H, d, *J*=9 Hz, H-2''), 4.50 (1H, s, H-5''), 4.41-3.36 (1H, dd, *J*=3 and *J*=12 Hz, H-5'), 4.12-3.93 (4H, m, H-6'/H-6''), 3.71-3.66 (1H, m, H-4'), 2.16-1.83 (21H, m, OC*H$_3$*) ppm. ^{13}C NMR ($CDCl_3$, 75.47 MHz) δ: 175.6 (C-9), 170.6-169.2 (7 *C*OCH$_3$), 163.2 (C-3/C-6), 158.0 (C-4a/C-10a), 128.5 (C-1/C-8), 116.4 (C-8a/C-9a), 113.5 (C-2/C-7), 101.5 (C-1''), 101.0

(C-4/C-5), 85.8 (C-1'), 77.4 (C-4'), 76.2 (C-5''), 75.9 (O-*C*H_2), 72.9 (C-3''), 72.3 (C-2''), 71.7 (C-3'), 70.5 (C-4''), 67.8 (C-2'/C-5'), 62.4 (C-6''), 61.7 (C-6') ppm.

4. CONCLUSION

In this project five compounds were successfully synthesized and purified, one of which is a new compound. The scale-up synthesis of gallic acid persulfate (**2**) gave an unexpected compound (**3**), with sulfate groups only on position 3 and 5.

Synthetic procedures using MW irradiation were successfully applied in the synthesis of sulfated derivative **3** and glucoside triazole-linked xanthones **9** and **11**. Regarding the structural elucidation, all compounds were characterized by IR, ^{1}H and ^{13}C NMR.

In the future, the antifouling activity will be tested for the new triazole linked xanthone possessing a disaccharide (**11**) to perform structure-activity relationship studies with the triazole linked xanthone monosaccharide (**9**) and consequently ponder the synthesis of more potent antifouling agents.

5. REFERENCES

1. Bixler, G.D. and B. Bhushan, *Biofouling: lessons from nature.* Philos. Trans. Royal Soc. A, 2012. **370**(1967): p. 2381-2417.
2. Phang, I.Y., et al., *Marine biofouling field tests, settlement assay and footprint micromorphology of cyprid larvae of Balanus amphitrite on model surfaces.* Biofouling, 2009. **25**(2): p. 139-147.
3. Magin, C.M., S.P. Cooper, and A.B. Brennan, *Non-toxic antifouling strategies.* Mater. Today, 2010. **13**(4): p. 36-44.
4. Cao, S., et al., *Progress of marine biofouling and antifouling technologies.* Sci. Bull., 2011. **56**(7): p. 598-612.
5. Poloczanska, E.S. and A.J. Butler, *Biofouling and climate change.* Biofouling, 2010. **333**.
6. Schultz, M.P., et al., *Economic impact of biofouling on a naval surface ship.* Biofouling, 2011. **27**(1): p. 87-98.
7. Bax, N., et al., *Marine invasive alien species: a threat to global biodiversity.* Mar. Policy, 2003. **27**(4): p. 313-323.
8. Bressy, C. and M. Lejars, *Marine fouling: an overview.* The Journal of Ocean Technology, 2014. **9**: p. 19-28.
9. Amara, I., et al., *Antifouling processes and toxicity effects of antifouling paints on marine environment. A review.* Environ. Toxicol. Pharmacol., 2018. **57**: p. 115-130.
10. Harremoës, P., et al., *Late lessons from early warnings: the precautionary principle 1896–2000.* 2001.
11. Gibbs, P.E., et al., *The use of the dog-whelk, Nucella lapillus, as an indicator of tributyltin (TBT) contamination.* J. Mar. Biol. Assoc. U. K., 1987. **67**(3): p. 507-523.
12. Dafforn, K.A., J.A. Lewis, and E.L. Johnston, *Antifouling strategies: history and regulation, ecological impacts and mitigation.* Mar. Pollut. Bull., 2011. **62**(3): p. 453-65.
13. Thomas, K. and S. Brooks, *The environmental fate and effects of antifouling paint biocides.* Biofouling, 2010. **26**(1): p. 73-88.

14. Jacobson, A.H. and G.L. Willingham, *Sea-nine antifoulant: an environmentally acceptable alternative to organotin antifoulants.* Sci. Total Environ., 2000. **258**(1): p. 103-110.
15. Gatidou, G., N.S. Thomaidis, and J.L. Zhou, *Fate of Irgarol 1051, diuron and their main metabolites in two UK marine systems after restrictions in antifouling paints.* Environ. Int., 2007. **33**(1): p. 70-77.
16. Dahms, H.U. and S. Dobretsov, *Antifouling compounds from marine macroalgae.* Mar. Drugs, 2017. **15**(9): p. 265.
17. Andersson Trojer, M., et al., *Imidazole and Triazole Coordination Chemistry for Antifouling Coatings.* J. Chem., 2013. **2013**: p. 23.
18. Nikapitiya, C., *Chapter 24 - Bioactive Secondary Metabolites from Marine Microbes for Drug Discovery*, in *Advances in Food and Nutrition Research*, S.-K. Kim, Editor. 2012, Academic Press. p. 363-387.
19. Lindequist, U., *Marine-Derived Pharmaceuticals – Challenges and Opportunities.* Biomol. Ther. (Seoul), 2016. **24**(6): p. 561-571.
20. Almeida, J.R., et al., *Antifouling potential of Nature-inspired sulfated compounds.* Sci. Rep., 2017. **7**: p. 42424.
21. Kurth, C., L. Cavas, and G. Pohnert, *Sulfation mediates activity of zosteric acid against biofilm formation.* Biofouling, 2015. **31**(3): p. 253-263.
22. Todd, J.S., et al., *The antifouling activity of natural and synthetic phenol acid sulphate esters.* Phytochemistry, 1993. **34**(2): p. 401-404.
23. Bauer, S., et al., *Adhesion of marine fouling organisms on hydrophilic and amphiphilic polysaccharides.* Langmuir, 2013. **29**(12): p. 4039-4047.
24. Callow, J.A. and M.E. Callow, *Trends in the development of environmentally friendly fouling-resistant marine coatings.* Nat. Commun., 2011. **2**: p. 244.
25. Wieland-Werke, A., *Corrosion, antifouling properties, fatigue and wear of copper alloys for seawater applications.* 2013.
26. Correia-da-Silva, M., et al., *Dual anticoagulant/antiplatelet persulfated small molecules.* Eur. J. Med. Chem., 2011. **46**(6): p. 2347-2358.
27. Al-Horani, R.A. and U.R. Desai, *Chemical Sulfation of Small Molecules – Advances and Challenges.* Tetrahedron, 2010. **66**(16): p. 2907-2918.
28. Brooke, L.T., W.-S. University of, and S. Center for Lake Superior Environmental, *Acute toxicities of organic chemicals to fathead minnows*

(Pimephales promelas). 1984, Superior, Wis., U.S.A.: Distributed by the Center.

29. Richard, M. and C. Alfred, *Ueber 3.6-Dioxyxanthon.* Ber. Dtsch. Chem. Ges., 1897. **30**(1): p. 969-973.
30. Wang, M.-L. and C.-Y. Yang, *Reaction mechanism of phase-transfer catalysis initiated by hydroxide ion: Effect of alkalinity.* Tetrahedron, 1999. **55**(20): p. 6275-6288.
31. Zhu, L., et al., *On the Mechanism of Copper(I)-Catalyzed Azide–Alkyne Cycloaddition.* Chem. Rec., 2016. **16**(3): p. 1501-1517.
32. Totobenazara, J. and A.J. Burke, *New click-chemistry methods for 1,2,3-triazoles synthesis: recent advances and applications.* Tetrahedron, 2015. **56**(22): p. 2853-2859.